Paleoceanography and Paleoclimatology

RESEARCH ARTICLE
10.1029/2020PA003934

Key Points:

- A synthesis of 67 tropical hydroclimate records from 55 sites indicate several regionally coherent patterns of change in the Common Era
- Robust patterns include a regional drying event from 800 to 1000 CE and a range of tropical hydroclimate changes ~1400–1700 CE
- Transient model simulations provide several new insights to the proxy reconstructions

Supporting Information:

Supporting Information may be found in the online version of this article.

Correspondence to:

A. R. Atwood,
aatwood@fsu.edu

Citation:

Atwood, A. R., Battisti, D. S., Wu, E., Frierson, D. M. W., & Sachs, J. P. (2021). Data-model comparisons of tropical hydroclimate changes over the Common Era. *Paleoceanography and Paleoclimatology*, *36*, e2020PA003934. https://doi.org/10.1029/2020PA003934

Received 6 APR 2020
Accepted 17 MAY 2021

Data-Model Comparisons of Tropical Hydroclimate Changes Over the Common Era

A. R. Atwood[1], D. S. Battisti[2], E. Wu[2], D. M. W. Frierson[2], and J. P. Sachs[3]

[1]Department of Earth Ocean and Atmospheric Science, Florida State University, Tallahassee, FL, USA, [2]Department of Atmospheric Sciences, University of Washington, Seattle, WA, USA, [3]School of Oceanography, University of Washington, Seattle, WA, USA

Abstract We examine the evidence for large-scale tropical hydroclimate changes over the Common Era based on a compilation of 67 tropical hydroclimate records from 55 sites and assess the consistency between the reconstructed hydroclimate changes and those simulated by transient model simulations of the last millennium. Our synthesis of the proxy records reveals several regionally coherent patterns on centennial time scales. From 800 to 1000 CE, records from the eastern Pacific and parts of Mesoamerica indicate a pronounced drying event relative to background conditions of the Common Era. In addition, 1400–1700 CE is marked by pronounced hydroclimate changes across the tropics, including dry and/or isotopically enriched conditions in South and East Asia, wet and/or isotopically depleted conditions in the central Andes and southern Amazon in South America, and fresher and/or isotopically depleted conditions in the Maritime Continent. We find notable dissimilarities between the regional hydroclimate changes and global-scale and hemispheric-scale temperature reconstructions, indicating that more work needs to be done to understand the mechanisms of the widespread tropical hydroclimate changes during the LIA. Apropos to previous interpretations of large-scale reorganization of tropical Pacific climate during the LIA, we do not find support for a large-scale southward shift of the Pacific Intertropical Convergence Zone, while evidence for a strengthened Pacific Walker Circulation and/or an equatorward contraction of the monsoonal Asian-Australian rain belt exists from limited geographic regions but require additional paleoclimate constraints. Transient climate model simulations exhibit weak forced long-term tropical rainfall changes over the last millennium but provide several important insights to the proxy reconstructions.

1. Introduction

The hydrologic cycle is expected to change in profound ways under continued increases in atmospheric greenhouse gas concentrations and yet our understanding of how regional rainfall patterns will respond to anthropogenic climate change remains highly uncertain. The short (spanning roughly half a century) and unevenly distributed precipitation records around the globe currently limit our ability to constrain models and thus make confident projections of future precipitation responses (Biasutti et al., 2018). However, the efficacy of the climate models used to project future climate can be tested against past records. In particular, the last 2,000 years, known as the Common Era, has been a major reconstruction target for the paleoclimate community over the last decade (Konecky et al., 2020; PAGES 2k Consortium, 2013, 2019; PAGES 2k-PMIP3 Group, 2015; Tierney et al., 2015) given its relative abundance of data and the similarity of the Earth's boundary conditions to present.

Global compilations of temperature reconstructions of the Common Era generally indicate a long-term cooling trend over the last millennium that extended into the middle of the 19th century, which was driven by increased volcanic activity (Atwood et al., 2016; Schurer et al., 2014), as well as solar, greenhouse gas, land use, and orbital forcings (Otto-Bliesner et al., 2016; Schurer et al., 2013; Swingedouw et al., 2011). Recent compilations of temperature-sensitive proxy data suggest that global mean surface temperatures cooled by ~0.2°C over the last millennium (PAGES 2k Consortium, 2013, 2019) with slightly larger cooling in the Northern Hemisphere (Hegerl et al., 2007; Mann et al., 2009; Marcott et al., 2013; Moberg et al., 2005) than the Southern Hemisphere (Neukom et al., 2014). Embedded within this global cooling trend, the Little Ice Age (LIA) is characterized as a period of regionally variable cooling during the second half of the last millennium ~1450–1850 CE (Cunningham et al., 2013; Kobashi et al., 2011; Masse et al., 2008; Neukom

et al., 2014; PAGES 2k Consortium, 2013). The spatial and temporal heterogeneity of the LIA reflects the complex array of forcings, feedbacks, and internal variability operating in the climate system at that time (Fernandez-Donado et al., 2013; Kaufman et al., 2009; Lehner et al., 2013). Evidence for amplified cooling in central Greenland (exceeding 1.0°C) has supported interpretations of Arctic amplified cooling during the LIA (Kobashi et al., 2011), which is also seen in transient climate model simulations of the last millennium (Atwood et al., 2016).

In the tropics, widespread changes in rainfall patterns are thought to have occurred during the LIA. In Asia, weakened summer monsoon rainfall and a prevalence of extreme droughts around 1300–1700 CE have been inferred from oxygen isotopes in cave deposits in India and China, from tree ring records from Southeast Asia, and from relative abundances of foraminifera from the Arabian Sea (Anderson et al., 2002; Buckley et al., 2010; Sinha et al., 2011; Wang et al., 2005; Zhang et al., 2008). Some studies have suggested that these rainfall changes contributed to the collapse of several major civilizations in India, China, and Southeast Asia (Buckley et al., 2010; Sinha et al., 2011; Zhang et al., 2008). On the opposite side of the Pacific basin in the Southern Hemisphere, an intensified South American summer monsoon ca. 1300–1500 CE and continuing through 1800 CE, has been inferred from records of oxygen isotopes in cave deposits, glacial ice, and authigenic calcite in lake sediments (Vuille et al., 2012).

Outside of these major monsoon systems, the nature of LIA hydroclimate changes in other regions of the tropics is more heavily disputed, particularly in and around the tropical Pacific Ocean. For example, different compilations of hydroclimate records from the Pacific basin and surrounding regions have been interpreted as representing either: (a) a southward migration of the mean annual position of the Pacific Intertropical Convergence Zone (ITCZ) (Nelson & Sachs, 2016; Richey & Sachs, 2016; Sachs et al., 2009) and Atlantic ITCZ (Haug et al., 2001), (b) an equatorward contraction of the Asian-Australian monsoons (Denniston et al., 2016; Griffiths et al., 2016; Yan et al., 2015), and/or (c) a strengthened Pacific Walker Circulation (Griffiths et al., 2016; Yan et al., 2011; Yan et al., 2015). Importantly, however, the definition of the LIA and the reference period varies widely across these studies; in some cases, the interpretation was based on trends during the LIA (e.g., Richey & Sachs, 2016), in other cases LIA conditions were referenced to the Medieval Climate Anomaly (MCA) in the early part of the last millennium (Haug et al., 2001; Nelson & Sachs, 2016) or to the modern period (Sachs et al., 2009), and in yet other cases, the MCA and modern periods were used interchangeably, depending on data availability (Yan et al., 2015). Standardizing these comparisons is critical to developing more robust constraints on the regional signatures of tropical hydroclimate changes during the last millennium.

Further complicating the interpretation of the LIA hydroclimate changes, theoretical frameworks to support the proposed rainfall changes are not well established. One theory links a southward migration of the zonal mean Hadley circulation to greater cooling of the Northern Hemisphere than the Southern Hemisphere during the LIA (Chiang & Bitz, 2005; Hwang et al., 2013; Kang et al., 2008). However, the applicability of this zonal mean energetic framework (i.e., the response of the zonal mean atmospheric circulation to changes in the hemispheric energy budget) to the regional scale of the paleoclimate records is unclear, given the relatively weak interhemispheric temperature changes during this time, and the evidence that shifts of the ITCZ are highly zonally variable even under a large interhemispheric asymmetry in forcing (Atwood et al., 2020; Roberts et al., 2017).

Over the past decade there has been a substantial increase in the number of high-resolution, hydroclimate-sensitive proxy records that are publicly accessible under improved paleo-data stewardship efforts. Here, we collect public data to reconstruct robust spatiotemporal patterns of tropical hydroclimate change over the Common Era using a larger suite of hydroclimate records than has previously been considered. Furthermore, we compare the reconstructed hydroclimate patterns to a large suite of transient climate model simulations of the last millennium to shed light on the mechanisms of the long-term hydroclimate changes, including distinguishing between forced and unforced modes of variability.

2. Materials and Methods

2.1. Proxy Record Selection and Treatment

Tropical hydroclimate records spanning the last millennium were selected from the NCDC/NCEI (https://www.ncdc.noaa.gov/) and PANGAEA (https://www.pangaea.de/) paleoclimate data repositories. A total of 67 speleothem, lake and marine sediment, and tropical glacier records were selected based on the following criteria: (a) the original authors interpreted the proxies as representative of hydroclimate conditions, (b) the records were located between 35°S and 35°N, and (c) the records spanned at least 70% of the last millennium (850–1850 CE) with a minimum temporal resolution of 200 years and contained at least one age control point within that period. More stringent record selection criteria were adopted for the cluster analysis and Empirical Orthogonal Function analysis, as detailed in Sections 2.2.1 and 2.2.3. For all analyses, the records were truncated outside of the time period 350–1950 CE and standardized to Z-scores by subtracting the mean and dividing by the standard deviation of the data during this interval. The Z-scores from each record (with zero mean and unit variance) were binned into 100-years windows to focus on the centennial to millennial-scale patterns in the data, and to limit the sensitivity of the results to the age model uncertainties in the reconstructions. The sign of the inferred relationship between rainfall amount and the measured values of the proxies was adopted from the original publication of each record. A lake minerology record from Kiritimati Atoll (Higley et al., 2018) was omitted from our analyses due to a substantial revision in the age model between 1200 CE and the core top (J. Conroy, personal communication). Table 1, Figure 1, and Table S1 provide a summary of the proxy records.

Of the 67 records in the compilation, 24% (16 out of 67) are nonwater isotope records, consisting of sediment grain size, bulk density, magnetic susceptibility, color, elemental composition (Ti/Ca, percent Mg in calcite), $\delta^{13}C$ of organic matter, and relative diatom abundances in lake and marine sediments (see Table S1). These archives are used to infer runoff intensity (which is related to the intensity, frequency, and/or amount of rainfall) and/or the local moisture balance. The remainder of the records (51 out of 67; 76%) are water isotope-based records, which reflect the isotopic composition ($\delta^{2}H$ or $\delta^{18}O$) of precipitation, groundwater, lake water, or near-surface seawater, and as such track numerous aspects of the hydrologic cycle. $\delta^{2}H$ and $\delta^{18}O$ records from closed lake systems generally reflect the local water balance of the lake (i.e., precipitation minus evaporation), while open lake, speleothem, and glacier ice records generally reflect the isotopic composition of precipitation, which integrates information about precipitation and evaporation rates, seasonality of precipitation, moisture sources, transport, and water recycling over land (Konecky et al., 2020). In the tropics, lower (higher) $\delta^{2}H$ and $\delta^{18}O$ values in meteoric water generally occur during periods of regionally wetter (drier) conditions, as described by the "amount effect," which is an empirical relationship in which the isotopic composition of precipitation in the tropics is negatively correlated with the amount of precipitation on monthly or longer time scales (Dansgaard, 1964; Risi et al., 2008). Reconstructions of surface seawater isotope ratios, meanwhile, provide a means of characterizing the surface exchange of freshwater and water mass mixing in the ocean, and therefore provide constraints on ocean salinity. While the data-model comparisons in this study are based on the assumption that the regionally coherent proxy signals are driven by regional changes in mean annual precipitation, future work should incorporate isotope-enabled model simulations that explicitly track water isotope ratios in the hydrosphere to provide more quantitative comparisons between the water isotope-based proxy records and model simulations.

2.2. Proxy Data Analyses

2.2.1. Hierarchal Cluster Analysis

Hierarchal cluster analysis (HCA; Eisen et al., 1998) was used to organize the paleoclimate records into groups with similar temporal patterns. In HCA, a binary, hierarchical cluster tree (dendrogram) links pairs of records that are in close proximity based on a specified distance metric; binary clusters are then grouped into larger clusters, forming a hierarchical tree. The height of the linkages in the dendrogram represents the distance between objects. HCA has been successfully used to divide diverse multiproxy paleoclimate data sets into groups with shared temporal patterns (Kaufman et al., 2016; Shuman et al., 2018). We constructed the hierarchical cluster tree in MATLAB (clusterdata.m) based on Euclidian pairwise distances between records and Ward's minimum variance method with a maximum of three clusters specified. For studies in

Paleoceanography and Paleoclimatology

10.1029/2020PA003934

Table 1
List of the Paleoclimate Data Used in This Study

Region	Site name	Lat (deg N)	Lon (deg E)	Elevation (m)	Proxy archive	Measurement	Cluster #, index #	Avg resolution (years)	Reference	Data set URL (if available)
Eastern Pacific	El Junco Lake, San Cristobal Island, Galápagos	−0.9	−89.5	670	Lake sediment	Dinosterol δ^2H	C1, 7	67	Atwood and Sachs (2014)	https://doi.org/10.1594/PANGAEA.834103
Eastern Pacific	El Junco Lake, San Cristobal Island, Galápagos	−0.9	−89.5	660	Lake sediment	Sediment grain size (% sand)	C1, 13	11	Conroy et al. (2008)	https://www.ncdc.noaa.gov/paleo/study/6109
Eastern Pacific	Poza de las Diablas, Isabela Island, Galápagos	−1.0	−91.0		Lake sediment	δ^2H lipid biomarkers	C1, 23	45	Nelson & Sachs (2016)	https://www.pnas.org/content/suppl/2016/03/09/1516271113.DCSupplemental
Central Pacific	Washington Island, Kiribati	4.7	−160.4		Lake sediment	δ^2H of total lipid extract		42	Sachs et al. (2009)	https://www.nature.com/articles/ngeo554#Sec11
South Pacific	Harai Lake #1, Rendova Island, Solomon Islands (SHAR1)	−8.6	157.4		Lake sediment	Dinosterol δ^2H		185	Maloney (2018)	–
South Pacific	Apu Bay, Tahaa, French Polynesia	−16.7	−151.5	0	Marine sediment	Ti/Ca	C1, 33	1	Toomey et al. (2016)	https://agupubs.onlinelibrary.wiley.com/doi/full/10.1002/2015PA002870
Maritime Continent	MD98-2181	6.3	125.8	−2114	Marine sediment	Carbonate $\delta^{18}O$ and Mg/Ca (forams)	C1, 40	34	Stott et al. (2004)	https://www.ncdc.noaa.gov/paleo/study/6236
Maritime Continent	Bukit Assam Cave, Malaysian Borneo	4.3	115.0	250	Speleothem	Carbonate $\delta^{18}O$		6	Chen et al. (2016)	https://www.ncdc.noaa.gov/paleo/study/19885
Maritime Continent	Snail Shell Cave, Malaysian Borneo (SSC01)	4.2	114.9	150	Speleothem	Carbonate $\delta^{18}O$	C3, 12	53	Carolin et al. (2016)	https://www.ncdc.noaa.gov/paleo/study/19806
Maritime Continent	MD98-2176	−0.2	133.4	−2382	Marine sediment	Carbonate $\delta^{18}O$ and Mg/Ca (forams)	C2, 41	42	Stott et al. (2004)	https://www.ncdc.noaa.gov/paleo/study/6236
Maritime Continent	Makassar Strait, Indonesia (31MC, 34GGC)	−3.9	119.5	−459 to −503	Marine sediment	δ^2H C30 fatty acid	C2, 32	33	Tierney et al. (2010)	https://www.ncdc.noaa.gov/paleo/study/10438
Maritime Continent	Makassar Strait, Indonesia (composite: 31MC, MD60, 34GGC, 32GGC)	−3.9	119.5	−454 to −503	Marine sediment	Carbonate $\delta^{18}O$ and Mg/Ca (forams)	C1, 26	10	Oppo et al. (2009)	https://www.ncdc.noaa.gov/paleo/study/8699
Maritime Continent	Makassar Strait, Indonesia (MD9821-60)	−5.2	117.5	−1185	Marine sediment	Carbonate $\delta^{18}O$ and Mg/Ca (forams)		9	Newton et al. (2006)	https://www.ncdc.noaa.gov/paleo/study/5534
Maritime Continent	Ranu Lamongan, East Java, Indonesia	−8.0	113.4	240	Lake sediment	Mol% Mg in calcite		3	Crausbay et al. (2006)	https://www.ncdc.noaa.gov/paleo/study/22409
Maritime Continent	Lake Lading, SW Indonesia	−8.0	113.3	324	Lake sediment	δ^2H n-alkanoic acid		9	Koneckey et al. (2013)	https://www.ncdc.noaa.gov/paleo/study/14129

Paleoceanography and Paleoclimatology

10.1029/2020PA003934

Table 1
Continued

Region	Site name	Lat (deg N)	Lon (deg E)	Elevation (m)	Proxy archive	Measurement	Cluster #, index #	Avg resolution (years)	Reference	Data set URL (if available)
Maritime Continent	Lake Logung, eastern Java, Indonesia	−8.0	113.3	215	Lake sediment	$\delta^{13}C$ of organic material	C2, 28	17	Rodysill et al. (2012)	https://www.ncdc.noaa.gov/paleo/study/8632
Maritime Continent	Liang Luar Cave, Flores, Indonesia (splice: LR06-B1, LR06-B3)	−8.5	120.4	550	Speleothem	Carbonate $\delta^{18}O$	C2, 16	12	Griffiths et al. (2009)	https://www.ncdc.noaa.gov/paleo/study/8632
Maritime Continent	MD98-2170	−10.6	125.4	−832	Marine sediment	Carbonate $\delta^{18}O$ and Mg/Ca (forams)		163	Stott et al. (2004)	https://www.ncdc.noaa.gov/paleo/study/6236
Australia	Cave KNI-51, Western Australia	−15.2	128.4	100	Speleothem	Carbonate $\delta^{18}O$		3	Denniston et al. (2016)	https://www.ncdc.noaa.gov/paleo/study/20530
South/East Asia	Huangye Cave, northern China	33.6	105.1	1650	Speleothem	Carbonate $\delta^{18}O$	C3, 30	5	Tan et al. (2010)	https://www.ncdc.noaa.gov/paleo/study/11177
South/East Asia	Jiuxian Cave, central China (C996-1)	33.6	109.1	1495	Speleothem	Carbonate $\delta^{18}O$	C2, 11	4	Cai et al. (2010)	https://www.ncdc.noaa.gov/paleo/study/9742
South/East Asia	Jiuxian Cave, central China (C996-2)	33.6	109.1	1495	Speleothem	Carbonate $\delta^{18}O$	C2, 11	27	Cai et al. (2010)	https://www.ncdc.noaa.gov/paleo/study/9742
South/East Asia	Wanxiang Cave, central China	33.3	105.0	1200	Speleothem	Carbonate $\delta^{18}O$	C3, 37	3	Zhang et al. (2008)	https://www.ncdc.noaa.gov/paleo/study/8629
South/East Asia	Sanbao Cave, central China (sb43)	31.7	110.4	1900	Speleothem	Carbonate $\delta^{18}O$		36	Dong et al. (2010)	https://www.ncdc.noaa.gov/paleo/study/10445
South/East Asia	Sanbao Cave, central China (sb26)	31.7	110.4	1900	Speleothem	Carbonate $\delta^{18}O$		26	Dong et al. (2010)	https://www.ncdc.noaa.gov/paleo/study/10445
South/East Asia	Heshing Cave, SW China	30.5	110.4	294	Speleothem	Carbonate $\delta^{18}O$	C1, 19	3	Hu et al. (2008)	https://www.ncdc.noaa.gov/paleo/study/6095
South/East Asia	Dongge Cave, southern China (D-4)	25.3	108.1	680	Speleothem	Carbonate $\delta^{18}O$	C1, 14	8	Dykoski et al. (2005)	https://www.ncdc.noaa.gov/paleo/study/5441
South/East Asia	Dongge Cave, southern China (DA)	25.3	108.1	680	Speleothem	Carbonate $\delta^{18}O$	C1, 35	4	Wang et al. (2005)	https://www.ncdc.noaa.gov/paleo/study/5439
South/East Asia	Dongge Cave, southern China (DX1)	25.3	108.1	680	Speleothem	Carbonate $\delta^{18}O$		1	Zhao et al. (2015)	ftp.ncdc.noaa.gov/pub/data/paleo/speleothem/Asia/China/Dongge2015.xls
South/East Asia	Xiang Yun Lake, China	24.4	102.8	1721	Lake sediment	Carbonate $\delta^{18}O$ (authigenic)	C3, 18	3	Hillman et al. (2014)	http://ncdc.noaa.gov/paleo/study/17515
South/East Asia	South China Sea	20.1	117.4	−1727	Marine sediment	Carbonate $\delta^{18}O$ (diatoms)	C2, 36	17	Wang et al. (1999)	https://www.ncdc.noaa.gov/paleo/study/2598
South/East Asia	Dandak Cave, India	19.0	82.0	400	Speleothem	Carbonate $\delta^{18}O$		1	Berkelhammer et al. (2010)	https://www.ncdc.noaa.gov/paleo/study/8639
South/East Asia	Jhumar Cave, India	18.9	81.9	600	Speleothem	Carbonate $\delta^{18}O$		2	Sinha et al. (2011)	https://www.ncdc.noaa.gov/paleo/study/11937

Paleoceanography and Paleoclimatology

10.1029/2020PA003934

Table 1
Continued

Region	Site name	Lat (deg N)	Lon (deg E)	Elevation (m)	Proxy archive	Measurement	Cluster #, index #	Avg resolution (years)	Reference	Data set URL (if available)
South/East Asia	Cattle Pond, Dongdao Island, South China Sea (DY2)	16.7	112.7		Lake sediment	Sediment grain size		14	Yan et al. (2011)	https://www.ncdc.noaa.gov/paleo/study/11197
South/East Asia	Cattle Pond, Dongdao Island, South China Sea (DY4)	16.7	112.7		Lake sediment	Sediment grain size		21	Yan et al. (2011)	https://www.ncdc.noaa.gov/paleo/study/11197
South/East Asia	Cattle Pond, Dongdao Island, South China Sea (DY6)	16.7	112.7		Lake sediment	Sediment grain size		6	Yan et al. (2011)	https://www.ncdc.noaa.gov
Africa	Lake Bosumtwi, Ghana	6.5	−1.4		Lake sediment	Carbonate $\delta^{18}O$ (authigenic)	C1, 29	5	Shanahan et al. (2009)	https://www.ncdc.noaa.gov/paleo/study/8657
Africa	Lake Edward, Uganda/ Democratic Republic of the Congo	−0.4	29.8	917	Lake sediment	% Mg in calcite		4	Russell et al. (2007)	https://figshare.com/articles/Proxy_data/4787575/1
Africa	Dante Cave, Namibia	−19.4	17.9		Speleothem	Carbonate $\delta^{18}O$		11	Sletten et al. (2013)	https://www.ncdc.noaa.gov/paleo/study/14268
Africa	Lake Sibaya, South Africa	−27.3	32.6	20	Lake sediment	% Planktonic diatoms	C2, 39	18	Stager et al. (2013)	https://www.ncdc.noaa.gov/paleo/study/14629
Mesoamerica	Tzabnah Cave, Yucatan, Mexico	20.7	−89.5	20	Speleothem	Carbonate $\delta^{18}O$	C1, 4	3	Medina-Elizalde et al. (2010)	https://www.ncdc.noaa.gov/paleo/study/9791
Mesoamerica	Lake Punta, Yucatan, Mexico	20.6	−87.5	14	Lake sediment	Carbonate $\delta^{18}O$ (Cytheridella ilosvayi)	C1, 1	7	Curtis et al. (1996)	https://www.ncdc.noaa.gov/paleo/study/5484
Mesoamerica	Lake Punta, Yucatan, Mexico	20.6	−87.5	14	Lake sediment	Carbonate $\delta^{18}O$ (Pyrgophorus coronatus)	C1, 1	7	Curtis et al. (1996)	https://www.ncdc.noaa.gov/paleo/study/5484
Mesoamerica	Laguna de Juanacatlán, Mexico	20.6	−104.7	2000	Lake sediment	Ti concentration		1	Metcalfe et al. (2010)	https://www.ncdc.noaa.gov/paleo/study/19768
Mesoamerica	Lake Chichancanab, Yucatan, Mexico	19.9	−88.8		Lake sediment	Lake sediment density	C1, 3	4	Hodell et al. (2008)	https://www.ncdc.noaa.gov/paleo/study/6108
Mesoamerica	Aguada X'caamal Lake, Yucatan Mexico	20.6	−89.7		Lake sediment	Carbonate $\delta^{18}O$ (Pyrgophorus coronatus)	C3, 2	4	Hodell et al. (2005)	https://www.ncdc.noaa.gov/paleo/study/6107
Mesoamerica	Lake Aljojuca, Mexico	19.1	−97.5	2376	Lake sediment	Carbonate $\delta^{18}O$ (authigenic)	C1, 8	18	Bhattacharya et al. (2015)	https://www.ncdc.noaa.gov/paleo/study/17735
Mesoamerica	Juxtlahuaca Cave, Mexico	17.4	−99.2	934	Speleothem	Carbonate $\delta^{18}O$	C2, 21	2	Lachniet et al. (2012)	https://www.ncdc.noaa.gov/paleo/study/12972
Mesoamerica	Peten-Itza Lake, Guatemala	17.0	−89.8	110	Lake sediment	Magnetic susceptibility	C2, 15	5	Escobar et al. (2012)	https://www.ncdc.noaa.gov/paleo/study/13675

Paleoceanography and Paleoclimatology

10.1029/2020PA003934

Table 1
Continued

Region	Site name	Lat (deg N)	Lon (deg E)	Elevation (m)	Proxy archive	Measurement	Cluster #, index #	Avg resolution (years)	Reference	Data set URL (if available)
Mesoamerica	Peten-Itza Lake, Guatemala	16.9	−89.8	110	Lake sediment	Carbonate $\delta^{18}O$ (Cochliopina sp.)		25	Curtis et al. (1998)	https://www.ncdc.noaa.gov/paleo/study/5482
Mesoamerica	Peten-Itza Lake, Guatemala	16.9	−89.8	110	Lake sediment	Carbonate $\delta^{18}O$ (Cytheridella ilosvayi)		14	Curtis et al. (1998)	https://www.ncdc.noaa.gov/paleo/study/5482
Mesoamerica	Peten-Itza Lake, Guatemala	16.9	−89.8	110	Lake sediment	Carbonate $\delta^{18}O$ (Pyrgophorus sp.)	C3, 5	12	Curtis et al. (1998)	https://www.ncdc.noaa.gov/paleo/study/5482
Mesoamerica	El Gancho Lake, Nicaragua	11.9	−85.9	44	Lake sediment	Carbonate $\delta^{18}O$ (ostrocod)		5	Stansell et al. (2012)	https://www.ncdc.noaa.gov/paleo/study/13195
South America	Cariaco Basin	10.7	−65.2	−893	Marine sediment	Ti concentration	C3, 17	5	Haug et al. (2001)	https://www.ncdc.noaa.gov/paleo/study/2560
South America	Laguna de Ubaque, Colombia	4.5	−73.9	2070	Lake sediment	% Lithics	C3, 10	10	Bird et al. (2017)	https://www.ncdc.noaa.gov/paleo/study/22275
South America	Laguna Pallcacocha, Ecuador	−2.8	−79.2	4200	Lake sediment	Red color intensity	C2, 22	0.5	Moy et al. (2002)	https://www.ncdc.noaa.gov/paleo/study/5488
South America	Laguna Pallcacocha, Ecuador	−2.8	−79.2	4200	Lake sediment	Greyscale	C1, 27	0.3	Rodbell et al. (1999)	https://www.ncdc.noaa.gov/paleo/study/5487
South America	Palestina Cave, Peru	−5.9	−77.4	870	Speleothem	Carbonate $\delta^{18}O$	C2, 38	3	Apaéstegui et al. (2014)	https://www.ncdc.noaa.gov/paleo/study/19301
South America	El Condor Cave, Peru	−5.9	−77.3	860	Speleothem	Carbonate $\delta^{18}O$		71	Cheng et al. (2013)	https://www.ncdc.noaa.gov/paleo/study/13836
South America	Tigre Perdido Cave, Peru (NC-A)	−5.9	−77.3		Speleothem	Carbonate $\delta^{18}O$	C2, 6	29	van Breukelen et al. (2008)	https://www.ncdc.noaa.gov/paleo/study/9790
South America	Cascayunga Cave, Peru	−6.1	−77.2	900	Speleothem	Carbonate $\delta^{18}O$		2	Reuter et al. (2009)	https://www.ncdc.noaa.gov/paleo/study/8630
South America	Lake Pumacocha, Peru	−10.7	−76.1	4300	Lake sediment	Carbonate $\delta^{18}O$ (authigenic)	C1, 9	2	Bird et al. (2011)	https://www.ncdc.noaa.gov/paleo/study/11174
South America	Huagapo Cave, Peru	−11.3	−75.8	3850	Speleothem	Carbonate $\delta^{18}O$	C1, 20	5	Kanner et al. (2013)	https://www.ncdc.noaa.gov/paleo/study/16405
South America	Diva de Maura, Brazil	−12.4	−41.6	680	Speleothem	Carbonate $\delta^{18}O$	C3, 24	5	Novello et al. (2012)	https://www.ncdc.noaa.gov/paleo/study/13670
South America	Quelccaya ice cap, Peru	−13.9	−70.8	5670	Glacial ice	Ice $\delta^{18}O$	C2, 31	10	Thompson et al. (2013)	https://www.ncdc.noaa.gov/paleo/study/14174
South America	Pau d'Alho Cave, Brazil	−15.2	−56.8		Speleothem	Carbonate $\delta^{18}O$	C1, 25	1	Novello et al. (2016)	https://www.ncdc.noaa.gov/paleo/study/20043

Table 1
Continued

Region	Site name	Lat (deg N)	Lon (deg E)	Elevation (m)	Proxy archive	Measurement	Cluster #, index #	Avg resolution (years)	Reference	Data set URL (if available)
South America	Cristal Cave, Brazil	−24.6	−48.6	130	Speleothem	Carbonate $\delta^{18}O$	C2, 34	2	Vuille et al. (2012) and Taylor (2010)	–

which more than one data set was generated to reconstruct hydroclimate at a given site, all relevant data sets from that study were averaged together. Records with missing data in more than two 100-years windows across the 350–1950 CE period of analysis were excluded from the cluster analysis; records with missing data in ≤ 2 windows were linearly interpolated and extrapolated. The Sletten et al. (2013) speleothem $\delta^{18}O$ record from Namibia and the Stansell et al. (2012) ostracod $\delta^{18}O$ record from Nicaragua were omitted to improve the stability of the cluster analysis. After these adjustments, 41 unique records remained in the cluster analysis. Composite records for each cluster were calculated by averaging all binned data from each cluster. The 95% confidence intervals were calculated based on 1,000 iterations of bootstrap sampling with replacement.

2.2.2. Regional Composites

In regions of high data density, regional composites of the proxy data were constructed to identify the robust regional hydroclimate signals in the reconstructions (Figure 1). Within each of the selected regions, regional composites were constructed from the Z-scores of the 100-years binned proxy data. For studies that invoked more than one data set to reconstruct hydroclimate at a given proxy site, the relevant data sets from that study were averaged together. Some records were omitted from the regional composites based on the original authors' interpretation of those records. In particular, we omitted the records from Laguna Pallacocha in the Ecuadorian Andes from the South American composite as these records were interpreted by the authors as representing ENSO-driven episodes of alluvial deposition, in contrast to the other records from this region.

2.2.3. EOF/PC Analysis

Empirical Orthogonal Function (EOF)/Principle Component (PC) Analysis was employed to characterize the dominant modes of variability in both the proxy records and models and to compare the patterns of variability between the proxies and models. These analyses were conducted on the full tropical data set, as well as on selected regional subsets of the data. The record selection criteria matched that of the cluster analyses in Section 2.2.1. To facilitate data-model intercomparison, the proxy data were truncated between 850 and 1850 CE, converted to Z-scores, and binned into 100-years windows (as in the cluster analysis) before calculating the PCs and EOF loadings. For the model simulations, precipitation and surface air temperature data from the individual models and ensemble and multimodel means were binned into 100-years windows to mimic treatment of the proxy data and the EOFs and PCs were calculated from regions bounded by the subsets of proxy data.

2.2.4. Epoch Analysis

The proxy reconstructions were compared to climate model output during the LIA and MCA epochs by averaging all data points in each standardized proxy record across the LIA (1450–1850 CE) and MCA (950–1200 CE). An unpaired two-sample Student's *t*-test was performed to assess the significance of the change between these time periods (with degrees of freedom equal to the number of data points in each epoch).

2.3. Model Simulations

We include two sets of model simulations in our analyses. The first set of simulations are six forced transient last millennium simulations that were performed in association with the Coupled Model Intercomparison Project Phase 5 (CMIP5)/Paleoclimate Intercomparison Project Phase 3 (PMIP3). These models are CCSM4 (Gent et al., 2011; Landrum et al., 2013); GISS-E2-R forcing ensemble members r1i1p121 and r1i1p124 (hereafter GISS 121 and GISS 124; Schmidt et al., 2006), which differ in their prescribed solar forcing, MPI-ESM-P (Marsland et al., 2003; Raddatz et al., 2007), CSIRO Mk3L version 1.2 (Phipps et al., 2012; Rotstayn et al., 2012), and HadCM3 (Collins et al., 2001; Pope et al., 2000; Schurer et al., 2013). The second set of simulations are from the Community Earth System Model (CESM) Last Millennium Ensemble (LME) version 1.1 (with version 5 of the Community Atmosphere Model; CAM5), consisting of a set of 13 experiments with all last millennium climate forcings included (orbital, volcanic, solar, and greenhouse gas), and the following single-forcing experiments: volcanic-only ($n = 5$), solar-only ($n = 4$), orbital-only ($n = 3$), greenhouse gas-only ($n = 3$), and land use only ($n = 3$), as detailed in Otto-Bliesner et al. (2016).

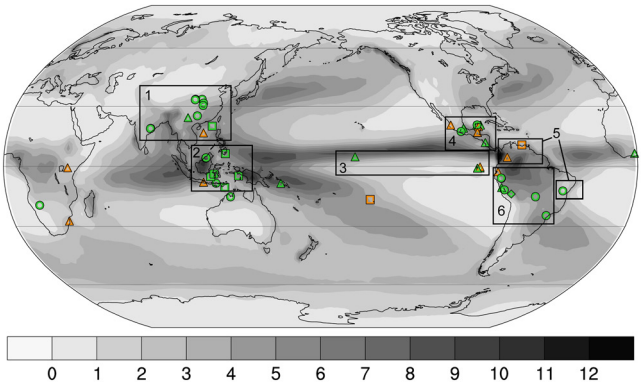

Figure 1. Observed mean annual precipitation from GPCP v.2.2 for the period 1979–2012 in mm/day. The location of the proxy records along with the archive type is denoted by the symbols (circle = speleothem, triangle = lake, square = marine sediment, and diamond = ice) and the color indicates whether the record is based on water isotopes (green) or not (orange). The numbered boxes enclose the proxy records that were used in the regional composites.

The prescribed forcings are described in Schmidt et al. (2011) and Otto-Bliesner et al. (2016); the volcanic and orbital forcings are also shown in Figures S1 and S2 of this study.

Two different reconstructions of volcanic aerosols and three different methods for implementing aerosols were used in the CMIP5/PMIP3 and CESM simulations analyzed in this study. The volcanic aerosol reconstructions were taken from either (a) the Gao et al. (2008) data set of stratospheric sulfate loading, where the loading is a function of month, latitude in 10 bands, and height from 9 to 30 km at 0.5-km resolution, or (b) the Crowley et al. (2008) data set of aerosol optical depth (AOD) (Schmidt et al., 2011). Substantial differences exist between the Gao et al. (2008) and Crowley et al. (2008) reconstructions with respect to the global mean and interhemispheric asymmetry of the aerosol forcing (Figure S1). The CCSM4 and CESM simulations prescribed sulfate loading from Gao et al. (2008), and stratospheric aerosols are prescribed in the models as a fixed single-size distribution in the three layers in the lower stratosphere above the tropopause (Landrum et al., 2013; Otto-Bliesner et al., 2016). The GISS 121, GISS 124, MPI, and HadCM3 simulations are forced by a prescribed aerosol effective radius and AOD from Crowley et al. (2008), which varies as a function of height and latitude in the atmosphere. In the CSIRO model, volcanic forcing was imposed as a globally averaged perturbation to total solar irradiance (TSI) that scales with the Crowley et al. (2008) data set of AOD (Masson-Delmotte, 2013).

2.4. Energy Budget Analysis

We quantified the hemispheric asymmetry of the forcings and feedbacks in the last millennium simulations during the LIA relative to the MCA by employing the Approximate Partial Radiative Perturbation (APRP) method (Taylor et al., 2007). The APRP method is based on a single-layer, shortwave radiative model of the atmosphere and has been successfully used to quantify the strength of climate forcings and feedbacks in a wide variety of paleoclimate, historical, and future climate simulations (e.g., Atwood et al., 2016; Crucifix, 2006; Hwang et al., 2013). In the APRP method, the influence of changes in surface albedo, shortwave absorption, and scattering on the TOA energy budget are diagnosed at every model grid cell using all-sky and clear-sky model output. Changes in the top-of-the-atmosphere (TOA) shortwave and longwave energy fluxes were decomposed into individual climate forcing and feedback terms as in Atwood et al. (2016), except that here the analysis is performed separately for each hemisphere. Energy fluxes are reported as NH minus SH, where negative terms indicate more NH energy loss (greater NH cooling) and positive terms indicate more SH energy loss (greater SH cooling). Radiation data for CSIRO and the CESM simulations were not available at the time of analysis and thus these simulations were omitted from the APRP analyses.

3. Results

3.1. Cluster Analysis of Proxy Records

The hierarchal cluster analysis indicates that the most common pattern, found in 41% of the tropical hydroclimate records analyzed, is a millennial-scale isotopic depletion trend beginning around 1000 CE and reversing around 1800 CE (Cluster 1 in Figures 2a and 2b), which generally tracks global temperature trends over the last millennium (Figure 3h; PAGES 2k Consortium, 2019). This cluster includes proxies from nearly every region represented in the proxy compilation (Figure 2c). We will demonstrate that this signal is not the dominant pattern in any regional compilation, however, and thus it likely does not reflect regional changes in precipitation. Instead, it may reflect global changes in the isotopic composition of water vapor (Falster et al., 2019), possibly driven by the cooling of tropical sea surface temperatures over the last millennium.

The next most common pattern, found in 37% of the records in the cluster analysis, including the majority of records from the Maritime Continent and the southwestern tropical South America (including the

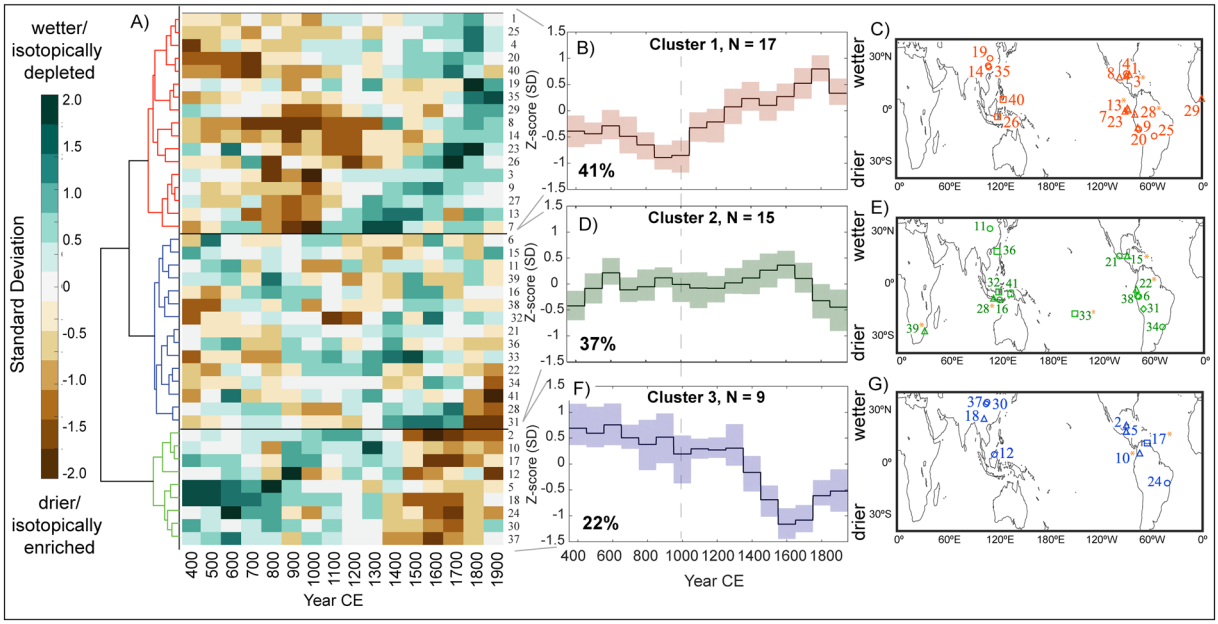

Figure 2. (a) Heat map and dendrogram from cluster analysis of standardized tropical hydroclimate records used in this study. (b, d, and f) Average (black line) and 95% bootstrap confidence intervals with 1,000 iterations (shading) of all records in each cluster. Proxy records were converted into Z-scores and averaged over 100-years bins during the period 350–1950 CE. For all records, higher Z-scores indicate wetter conditions, based on interpretation in the original study from Table 1. (c, e, and g) Location of proxy records, where the symbols correspond to the type of proxy archive indicated in Figure 1. Symbols with a yellow asterisk indicate that the record is not based on water isotopes.

central Andes and the southern Amazon), is dominated by a drying (and/or isotopic enrichment) trend from 1600 CE to present (Cluster 2; Figures 2d and 2e). An opposing trend is observed in the third cluster, which contains 22% of the records, including those from northern and eastern South America, and parts of Mesoamerica and East Asia (Cluster 3; Figures 2f and 2g). In this cluster, the dominant pattern is drying (and/or isotopic enrichment) beginning ca. 1300 CE and peaking during the LIA around 1600–1700 CE, followed by a wetting trend to present.

3.2. Regional Composites of Proxy Records

When the records are compiled by region, several robust regionally coherent hydroclimate patterns emerge that provide more insight into the patterns found in the cluster analysis. From 800 to 1000 CE, encompassing the early part of the MCA, three lake records from two islands in the eastern equatorial Pacific indicate notably dry (and/or isotopically enriched) conditions relative to the average over the Common Era (Figure 3a), a pattern that is also found in half (5/10) of the records from Mesoamerica, especially those clustered in the northern part of the region (Figure 3b). The remaining 5/10 Mesoamerican records, which extend father south, indicate a distinctly different centennial pattern, characterized by a steady drying (and/or isotopic enrichment) trend from 1200 CE to present (Figure 3c).

During the second half of the last millennium, records from the major monsoon systems of Asia and South America demonstrate antiphased behavior. In South and East Asia, nearly all records demonstrate anomalously dry (and/or isotopically enriched) conditions ca. 1400–1700 CE followed by a coherent wetting (and/or isotopic depletion) trend to present (Figure 3f). In contrast, nearly all records from the central Andes and Southern Amazon in South America indicate anomalously wet (and/or isotopically depleted) conditions ca. 1500–1700 CE, followed by a drying trend to the present (Figure 3e). During the LIA, the South American records are characterized by an opposing pattern between the southern/western sites and the northern/eastern sites: southwestern South America experienced a wetting (and/or isotopic depletion) trend from 1300 to 1600 CE while northern South America and Nordeste Brazil experienced a drying (and/or isotopic enrichment) trend (Figures 3d and 3e). From 1600 CE to present, northern South America and Nordeste Brazil remained anomalously dry while southwestern South America experienced a drying trend.

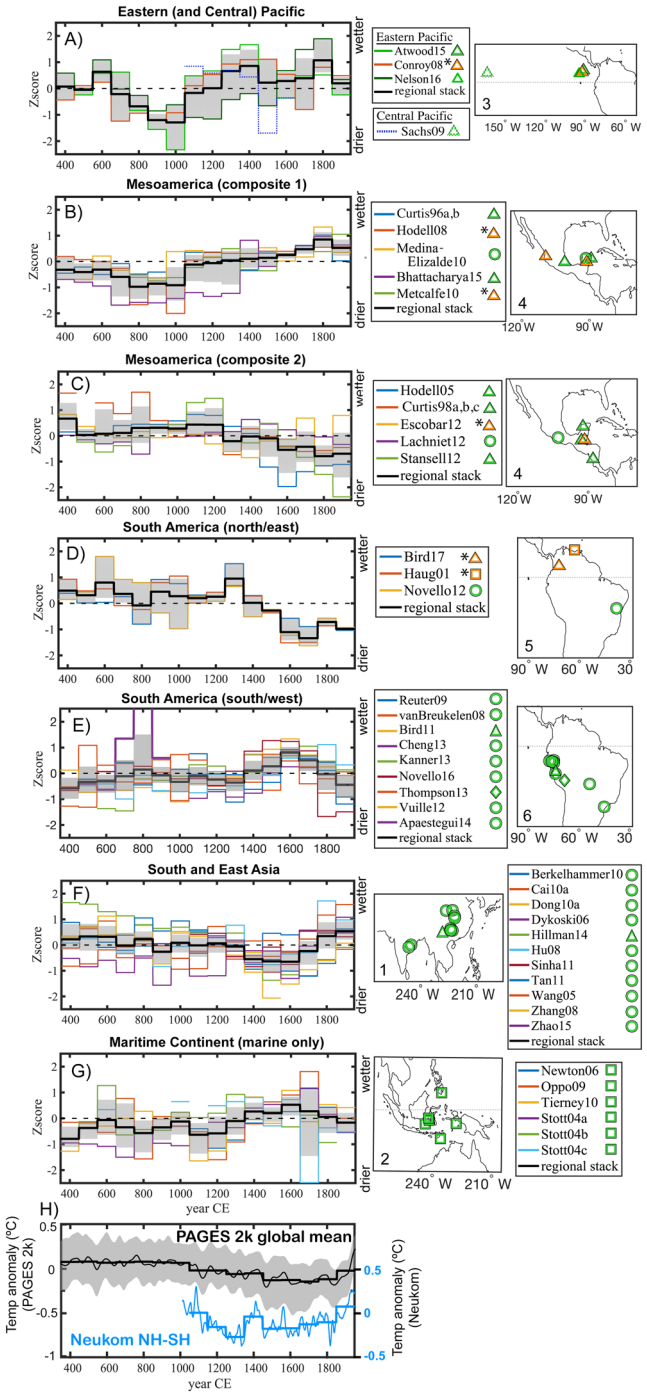

Figure 3. (a–g) Regional compilations of the tropical hydroclimate records, converted into Z-scores and averaged over 100-years bins. For all records, higher Z-scores indicate wetter conditions, based on interpretation in the original study (from Table 1). The average and standard deviation of all records in each region are depicted by the black line and shading, respectively. The maps indicate the location of the records, where the symbol denotes the type of proxy archive (circle = speleothem, triangle = lake, square = marine sediment, diamond = ice) and the color indicates whether the record is based on water isotopes (green) or not (orange with asterisk). The legend indicates the relevant reference for each record (see Table 1). Overlapping symbols have been slightly offset for visual clarity. (h) The reconstructed global mean temperature anomaly (relative to 1000–1200 CE) from PAGES 2k Consortium (2019) is shown in black, where the solid line is the 31-year low-pass filtered ensemble median, and the shading is the 2.5th and 97.5th percentiles of all reconstruction members; the Neukom et al. (2014) reconstructed interhemispheric (NH-SH) temperature difference is shown in blue (30-years loess-filtered ensemble mean). The averages over 100-years bins are also shown for both temperature reconstructions.

Hydroclimate records from the Maritime Continent generally oppose the hydroclimate patterns observed in Asia. Namely, the composite of marine records from the Maritime Continent indicates isotopically depleted precipitation and seawater (and by inference lower salinity) from 1500 to 1700 CE (Figure 3g), followed by an isotopic enrichment trend to present. The coherence is especially pronounced in the four marine records from the Makassar Strait and south of the Philippine Islands (Figure S3d). A single speleothem record from northern Australia reflects the Asian monsoon trends to some extent, with drier (and/or isotopically enriched) conditions ca. 1400–1600 CE, relative to much of the prior 500 years, followed by a wetting (and/or isotopic depletion) trend to present (Figure S3c). These features provide some evidence of coherence between the northern and southern margins of the Asian-Australian rain belt. However, while the LIA conditions in Asia are anomalous with respect to the average conditions of the Common Era, this is not the case for the northern Australia record. Additional hydroclimate records from northern Australian are needed to confirm the regional patterns in this area, as only a single record that spanned the last millennium was publicly available at the time of analysis.

3.3. Simulated Tropical Precipitation Changes Over the Last Millennium

To investigate the mechanisms of the robust hydroclimate changes inferred from the proxy records, including distinguishing between forced and unforced variability, we compared the reconstructions to a large suite of transient climate model simulations of the last millennium. The forced response of tropical rainfall is weak on centennial time scales in the models, as indicated by the small (<10%) LIA precipitation changes relative to the models' climatology in the CMIP5/PMIP3 multimodel mean (Figure 4b) and in the CESM ensemble mean (Figure 4d). The weak forced responses are due to large differences in tropical rainfall anomalies during the LIA across different models (Figure S4a) and across different ensemble members of the same model (CESM; S4b).

However, the precipitation changes in the CMIP5/PMIP3 multimodel average show several areas of broad agreement with the ensemble average changes in CESM (Figure 4), suggesting similar forced precipitation responses across models in these regions. For example, during the LIA relative to the MCA, nearly all CMIP5/PMIP3 models and all CESM ensemble members simulate large-scale drying in South and East Asia, drying over the Sahel, wetting in the equatorial Atlantic Ocean that extends to the northeastern edge of South America, drying along the southwestern edge of the South Pacific Convergence Zone, and large-scale drying of the midlatitudes and high latitudes (Figure S4). These features are qualitatively similar between the first and second half of the LIA, but are more pronounced in the second half of the LIA (Figure S5). The CESM single-forcing experiments indicate that these tropical rainfall changes are largely driven by orbital forcing in the models, with drying over Asia and wetting along the northeast coast of South America also driven by volcanic forcing (Figure 5). Further details of the tropical hydroclimate responses to orbital forcing are provided in the supporting information (Text S1). Notably, in tropical South America, the models do not simulate a strengthening of the South American Summer Monsoon (SASM) during the LIA, and few coherent rainfall changes occur over South America in the simulations during the height of the monsoon season in austral summer (DJF; Figures S6a and S6c).

In the tropical Pacific, the precipitation changes are notably different between the CESM ensemble average and CMIP5/PMIP3 multimodel average, tracking differences in the tropical cooling patterns in the two sets of model simulations over the last millennium (Figure S7). Namely, the CMIP5/PMIP3 multimodel mean precipitation response features a robust meridional pattern, with drying in the northern branch of the Pacific ITCZ, while the northern subtropical Pacific and southeastern Pacific become wetter, consistent with a weakened local Hadley circulation in this region (Figures 4 and S7a). This meridional rainfall pattern is consistent with the change in tropical surface temperatures which features enhanced cooling in the northern tropical Pacific, including under the northern branch of the Pacific ITCZ (Figure S7b). In contrast, the forced precipitation trend in the CESM simulations features an enhanced Pacific Walker Circulation, with drying in the central and eastern equatorial Pacific that extends all the way to the far western Pacific (Figures S7c and S7d). The internal variability in the Indo-Pacific is generally larger than the forced signal in CESM however (Figure S8), and thus the long-term strengthening of the Walker circulation is only weakly significant (see the lack of stippling in much of the Indo-Pacific in Figures 4c and 4d). The internal variability is characterized by centennial variations in the Walker Circulation with a node in the precipitation

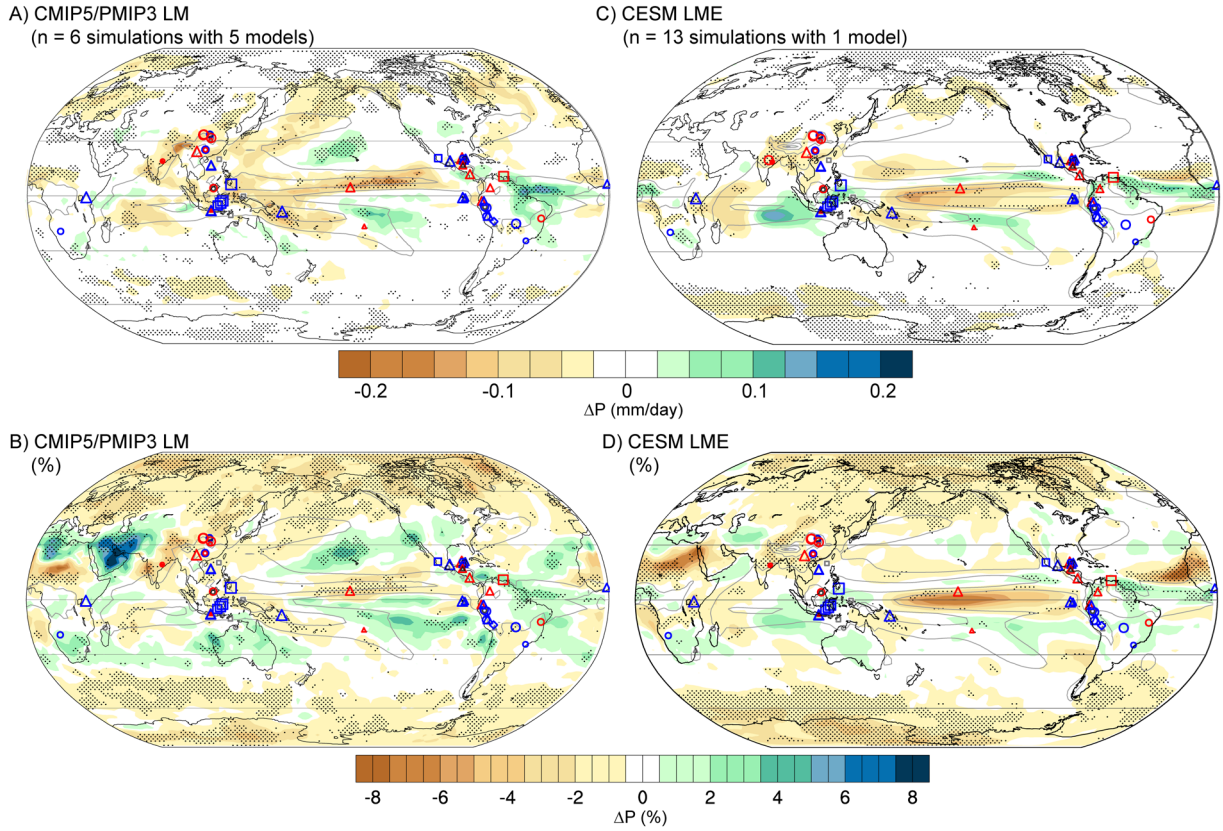

Figure 4. Multimodel mean change in precipitation during the Little Ice Age (LIA, 1450–1850 CE) relative to the MCA (950–1200 CE). (a and b) ΔP in the six Paleoclimate Intercomparison Project Phase 3 (PMIP3)/Coupled Model Intercomparison Project Phase 5 (CMIP5) LM simulations in units of (a) mm/day and (b) percent, relative to mean annual precipitation during the Medieval Climate Anomaly (MCA). (c and d) ΔP in the 13 all-forcing Community Earth System Model (CESM) LME simulations in units of (c) mm/day and (d) percent, relative to mean annual precipitation during the MCA. Unfilled contours are mean annual precipitation during the MCA (with contours at 4 and 8 mm/day). Stippling indicates where ≥83% of the models agree on the sign of the change (5/6 models in panels a, b and 11/13 simulations in panels c, d). The markers indicate the paleo-hydroclimate records in Table 1, where the type of symbol denotes the proxy archive (circle = speleothem, triangle = lake sediment, square = marine sediment, diamond = ice), the size of the marker scales with log of the difference in Z-scores, and the color represents the sign of the inferred precipitation change (blue = positive/wetter, red = negative/drier, gray = no significant change) during the LIA relative to the MCA, based on an unpaired two-sample Student's *t*-test.

anomalies near the date line, while the forced response is characterized by a weak enhancement of the Walker Circulation with a drying trend that extends farther west and wetting in the Maritime Continent west of Papua New Guinea (Figure S8). The forced response in CESM is driven by a combination of forcings: orbital and volcanic forcing drive an enhanced Pacific Walker Circulation, while land use forcing drives drying in the far western Pacific (Figure 5). However, this tropical Pacific response to the last millennium forcings appears to be unique to CESM since none of the CMIP5/PMIP3 models simulate a strengthening of the Walker Circulation over the last millennium (Figures S4 and 6; though multiple ensemble members of the CMIP5/PMIP3 simulations would be required to identify the true forced response in those models). In CESM, the forced response and the large unforced centennial variations in the Walker Circulation may be related to stronger tropical Pacific ocean-atmosphere coupling in that model, as suggested by the larger interannual to centennial climate variability in the tropical Pacific in the CESM last millennium simulations as compared to the CMIP5/PMIP3 last millennium simulations (Figure S10). The magnitude of tropical Pacific climate variability varies widely across models, ranging from weak variability in the GISS and CSIRO last millennium simulations, in which the variance of Niño 3 SST anomalies is around 30% of that observed over the last 40 years, to large variability in CESM, in which the variance of Niño 3 SST anomalies is around 150% of that observed (Figure S11).

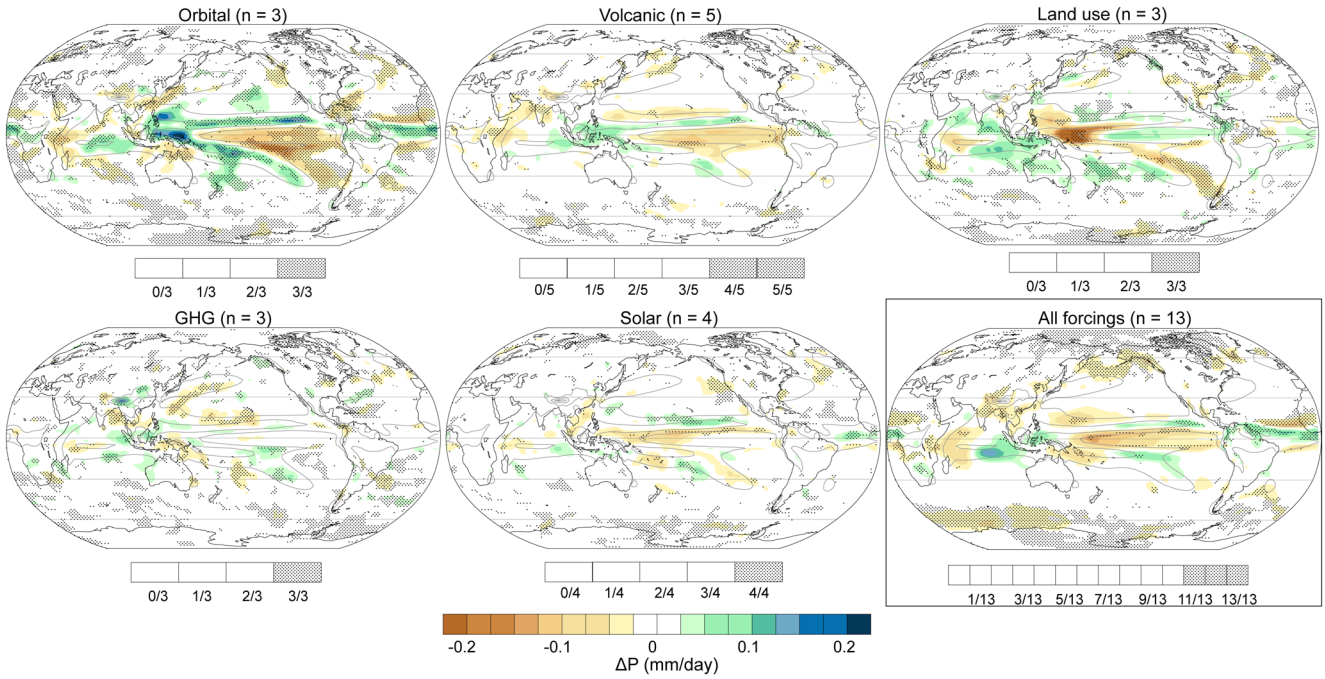

Figure 5. Ensemble mean precipitation change (colors) in the CESM individual forcing simulations during the LIA (1450–1850 CE) relative to the MCA (950–1200 CE). Unfilled contours indicate the mean annual precipitation during the MCA (contours are 4 and 8 mm/day). Stippling indicates where ≥80% of the ensemble members agree on the sign of the change (as shown in the shaded bar below each subplot).

3.4. Data-Model Intercomparison

Point-to-point comparisons between the proxy data and models are generally not meaningful because of the structural uncertainties in simulated precipitation climatology associated with the coarse spatial resolution and large tropical mean state biases in the models (e.g., PAGES Hydro2k Consortium, 2017). In addition, most of the proxy records included in this analysis are based on water isotopes, hence they record regional, as well as local, hydroclimate variations. For these reasons, we focus on comparing the proxy records to simulated precipitation over a regional scale.

The simulations highlight three large-scale hydroclimate features that are worthy of consideration when interpreting the proxy records. The first is the large-scale drying pattern over South and East Asia from the MCA to LIA, which appears in both the proxies and models (Figure 4) and is driven by volcanic and orbital forcing in CESM (Figure 5). Importantly, however, the temporal evolution of the drying trend from the LIA to present is notably different between the models and proxies; this distinction becomes more evident when an EOF analysis is performed only on the Asian records and precipitation fields (Figure S12). The proxy data (comprised of Asian speleothem and lake sediment records) features a coherent drying trend that peaks around 1600 CE, followed by a reversal (wetting trend) through 1850 CE (Figure S12a). In contrast, the models, particularly the CMIP5/PMIP3 models, are characterized by a persistent drying trend over Asia through the last millennium and enhanced drying from 1600 to 1850 CE (Figures S12b and S12c).

A second large-scale hydroclimate feature in the models that may be relevant to the proxy reconstructions is increased rainfall in the South American monsoon entrance region, upstream of the SASM. The proxy records in the central Andes and southern Amazon indicate isotopically depleted conditions ca. 1500–1700 CE, consistent with a greater degree of upstream rainout (Vuille & Werner, 2005). Contrary to previous interpretations of the South American proxy records (e.g. Vuille et al., 2012), there is no indication of enhanced SASM activity in the models, however, precipitation increases in the equatorial Atlantic and extends into the monsoon entrance region in nearly all models (Figures 4 and S4), driven by orbital and volcanic forcing in CESM (Figure 5). Under orbital forcing, the increase in equatorial Atlantic rainfall occurs alongside a contraction in the Atlantic ITCZ (i.e., a reduced seasonal migration of the Atlantic ITCZ), which we discuss in more detail in Section 4.3.3.

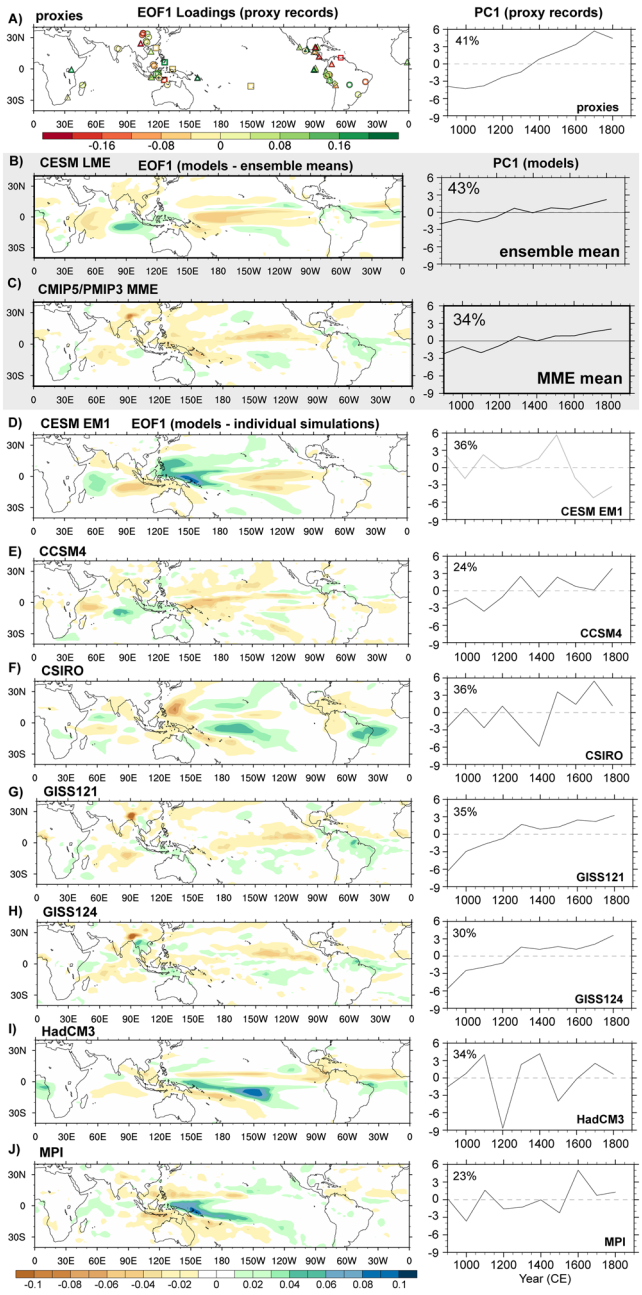

Figure 6. Normalized EOF 1 loadings and PC 1 of (a) the proxy Z-scores, (b) simulated tropical precipitation in the CESM ensemble mean, (c) simulated tropical precipitation in the CMIP5/PMIP3 multimodel mean, and (d–h) simulated tropical precipitation in the first ensemble member of the CESM LME and in each of the CMIP5/PMIP3 last millennium simulations. The proxy and model data were binned into 100-years windows prior to EOF analysis. Higher values of the loadings indicate wetter (or more isotopically depleted) conditions.

The third large-scale hydroclimate feature is shared between the proxy data and select CESM simulations. This feature is characterized by wetter LIA conditions in the Maritime Continent coupled with dry conditions in the central tropical Pacific (Figures 4 and S4). In CESM, this feature is associated with an enhanced Pacific Walker Circulation and occurs in 8/13 ensemble members (Figure S4; Figure S8) and also occurs in the ensemble mean response (Figure 4). In the proxies, evidence of this feature exists in the Maritime Continent records and in the single central Pacific record; but is notably lacking in the eastern equatorial Pacific records where there is pronounced data-model mismatch (the three records from the Galápagos Islands indicate wetter conditions during the LIA, while the models indicate drying or no change; Figures 4 and 3a). Thus, additional hydroclimate records from the Pacific cold tongue are needed to support any inference of a change in the Pacific Walker Circulation during the LIA.

3.5. Small but Robust Zonally Averaged Tropical Rainfall Response in Models

Despite large differences in regional precipitation across models, some coherence is observed in the zonally averaged context: all models demonstrate a small zonal mean southward shift in tropical precipitation (20°S:20°N) during the LIA relative to the MCA (Figure 7). The change in the precipitation asymmetry ($\Delta P_{NH\text{-}SH}$; the precipitation averaged between 0°N and 20°N minus 0 and 20°S) is small (≤0.3 mm/day), representing a −15% to +10% change in precipitation asymmetry across models. To put the magnitude of these changes into context, the multimodel mean change in the tropical precipitation centroid (defined as the median of zonal average precipitation from 20°S to 20°N) is −0.03° latitude in the last millennium simulations (data not shown), which is 6% as large as the −0.53° multimodel mean shift in the PMIP2 and PMIP3 Last Glacial Maximum simulations and 1% as large as the −2.48° shift in 1 Sv North Atlantic meltwater simulations (Atwood et al., 2020).

This robust zonal mean precipitation shift occurs in association with anomalous northward cross-equatorial atmospheric energy transport in all models that is primarily driven by volcanic forcing (i.e., greater volcanic aerosol loading in the northern hemisphere) and land use changes (i.e., cropland expansion in Eurasia), and is amplified by the surface albedo feedback (e.g., through the growth of Arctic sea ice in response to orbital forcing) and longwave feedbacks (Figure S13). While these zonal mean changes are small ($\Delta P_{NH\text{-}SH} \leq 0.3$ mm/day; $\Delta AHT_{\Phi=0} < 0.2$ W/m^2), they demonstrate a perceptible influence of the hemispherically asymmetric forcings (namely volcanic forcing and Eurasian cropland expansion) and feedbacks (e.g., the surface albedo feedback) on the zonal mean tropical precipitation response in the models. Additional details of the energy budget analysis can be found in the supporting information (Text S2).

The fact that the zonal mean precipitation changes are fairly consistent across models indicates that the net hemispheric asymmetry in the forcings and feedbacks are generally consistent across models and also indicates that the zonal mean precipitation response is less sensitive to structural uncertainties in the models than the regional rainfall responses are. However, the zonal mean rainfall changes are clearly irrelevant to our analysis of regional rainfall patterns, since they are too small to be of consequence for interpreting the

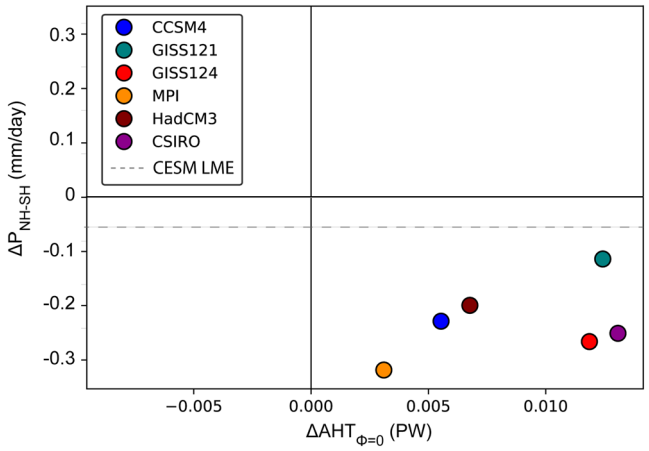

Figure 7. Change in zonal mean interhemispheric tropical precipitation asymmetry between 20°S:20°N ($\Delta P_{NH\text{-}SH}$) in the LIA (1450–1850 CE) relative to the MCA (950–1200 CE) versus the change in cross-equatorial atmospheric energy transport ($\Delta AHT_{\Phi=0}$) in the PMIP3/CMIP5 last millennium simulations. Positive values of $\Delta AHT_{\Phi=0}$ represent anomalous northward heat transport. $\Delta P_{NH\text{-}SH}$ averaged over the 13-member CESM last millennium ensemble is shown by the dashed horizontal line (the radiation data needed to calculate $\Delta AHT_{\Phi=0}$ was not obtained for the CESM LME).

changes seen in the proxy records and since zonal mean changes have little bearing on regional rainfall patterns (e.g., Atwood et al., 2020).

4. Discussion

Three robust signatures of tropical hydroclimate change over the Common Era have emerged from our analyses of the centennial patterns in the proxy records. These are: (a) a pan-tropical isotopic depletion trend in the water isotope-based records over the past millennium (Cluster 1), (b) anomalously dry conditions in the eastern tropical Pacific Ocean and Mesoamerica between 800 and 1000 CE, and (c) a range of widespread hydroclimate anomalies across the tropics from 1400 to 1700 CE, including drier and/or isotopically enriched conditions in South and East Asia, wetter and/or isotopically depleted marine conditions in the Maritime Continent, and a dipole pattern in South American hydroclimate. We discuss each of these robust regional patterns in more detail below.

4.1. Isotopic Depletion Trend in Pan-Tropical Records Over the Last Millennium

The dominant pattern of centennial hydroclimate variability, found in 41% of the tropical hydroclimate records analyzed (14 out of 17 of which are based on water isotopes) and appearing in nearly every region of the tropics represented in the proxy compilation, is an isotopic depletion trend beginning around 1000 CE and reversing around 1800 CE (Figures 2a–2c) (Falster et al., 2019), which tracks global temperature trends over the Common Era (Figure 3h; PAGES 2k Consortium, 2013, 2019). In model simulations, global cooling of 0.2°C–0.3°C over the last millennium (Figure S14a) is accompanied by a perceptible but very weak decrease in tropical area-averaged precipitation (Figure S14b; $\Delta P_{LIA\text{-}MCA} = -0.28 \pm 0.08\%$ [1σ] and $-0.23 \pm 0.04\%$ for the CMIP5/PMIP3 and CESM runs, respectively). However, the magnitude of these precipitation changes would be far too small to be detectable in nonwater isotope-based proxy archives (which indirectly reflect changes in precipitation), or in water isotope-based records via the amount effect. Water isotope tracers, however, are sensitive to both precipitation and evaporative fluxes (the latter of which supply the atmospheric water vapor reservoir from which all precipitation is derived). Thus, the millennial-scale isotopic depletion trend observed in many of the proxy records is likely not associated with changes in precipitation, but rather with decreased evaporation rates (and increased fractionation during evaporation) under cooler tropical sea surface temperatures (Risi, Bony, Vimeux, & Jouzel, 2010). This hypothesis is supported by the models' robust pan-tropical cooling trend over the last millennium (Figures S8 and S9) and is currently being explored using model simulations with water isotope tracers (Falster et al., 2019). The response of the global water cycle to cooling over the last millennium—and how those changes are recorded in water isotope tracers—is worthy of further investigation using such tools.

4.2. Dry Conditions in the Eastern Pacific and Mesoamerica ~800–1000 CE

One of the robust regional hydroclimate signals to emerge from our analysis is the pronounced drying event from 800 to 1000 CE recorded in a series of lake sediment records from the Galápagos Islands in the eastern equatorial Pacific (Figure 3a; 1°S, 90–91°W) and in many lake and speleothem records from Mesoamerica (Figure 3b). This signal is evident in a variety of different types of paleo-hydroclimate archives, including minerology and water isotope-based records from lake sediments as well as speleothem records, suggesting a common mechanism of regional precipitation changes in these regions. This event is apparent in the regional composites from the eastern equatorial Pacific (Figure 3a) and northern Mesoamerica (Figure 3b) as well as in the cluster analysis (Figures 2a–2c). Evidence of a pronounced drying event during this interval has also been found in a sediment minerology record from a brackish lake in Kiritimati Atoll in the central equatorial Pacific (Higley et al., 2018).

A period of extended drought across Mesoamerica from 800 to 1050 CE has been inferred in earlier studies and implicated in major social disruptions in pre-Columbian Mesoamerican civilizations (e.g., Bhattacharya et al., 2017; Hodell et al., 2005). The consistency in timing between the dry intervals in Mesoamerica and the tropical Pacific cold tongue is suggestive of a dynamical linkage between the eastern Pacific climatology and the Mesoamerican monsoon during this time.

4.3. Widespread Tropical Hydroclimate Changes During the LIA ~1400–1700 CE

The second half of the last millennium is characterized by a set of widespread, nearly synchronous hydroclimate changes throughout the tropics from 1400 to 1700 CE, including: (a) isotopically enriched (drier) conditions in South and East Asia, (b) isotopically depleted (fresher) surface ocean conditions in the Maritime Continent, and (c) a dipole pattern in tropical South America. We investigate each of these regional signals and discuss their possible interpretations, below.

4.3.1. Dry/Isotopically Enriched Conditions in South and East Asia

Hydroclimate reconstructions from South and East Asia generally indicate isotopically enriched (drier) conditions from 1400 to 1700 CE relative to present and to the background conditions of the Common Era, followed by progressively depleted (wetter) conditions to present (Figure 3f). LIA drying in this region is also apparent in the LIA-MCA epoch analysis (Figure 4), and in the EOF/PC analysis (Figure S12a). Because all of the proxy records from Asia are water isotope records (10 speleothem $\delta^{18}O$ records and one lake carbonate $\delta^{18}O$ record) (Figure 3f), which integrate climate information on large spatial scales, the widespread signature of isotopic enrichment in these records likely reflects reduced upstream rainout associated with a weakened South, and possibly East Asian, monsoon during the LIA.

This interpretation is consistent with past studies that have characterized the LIA as a time of weakened South and East Asian summer monsoon strength, marked by a series of monsoon droughts in India, China, and Southeast Asia (Sinha et al., 2011; Zhang et al., 2008). Proposed mechanisms for the weakened monsoons include widespread extratropical NH cooling that drove a southward shift of the rain belt in the Indian Ocean (Sinha et al., 2011) and reduced land-sea temperature contrast between Asia and the tropical Indo-Pacific (Zhang et al., 2008). We do indeed see weakening of the South and East Asian monsoons over the last millennium in the models under enhanced cooling over land, particularly in the NH, that is driven by orbital and volcanic forcing (Figures 4, 5, and S7). However, the temporal pattern of the changes is notably different between the reconstructions and models. In the reconstructions, aridity in the Asian records peaks around 1600 CE, followed by a wetting trend to the present era, while in the models, the drying trend extends to at least 1800 CE (Figure S12). Thus, though the models indicate that the weakening of the Asian monsoons during the LIA may have been driven in part by orbital and/or volcanic forcing, there are clear limitations in the models' ability to capture this important feature of tropical hydroclimate change over the last millennium.

4.3.2. Wet/Isotopically Depleted Conditions in the Maritime Continent

Further evidence that the period from 1400 to 1700 CE was characterized by widespread tropical hydroclimate changes comes from the Maritime Continent. In this region, marine records generally indicate isotopically depleted precipitation and surface ocean conditions around 1400–1700 CE, relative to present and to the background conditions over the Common Era (Figure 3g). One of the six marine records is a hydrogen isotope leaf wax record from the West Sulawesi margin, which is a proxy for the isotopic composition of precipitation in the region (Tierney et al., 2010). The remaining records are seawater $\delta^{18}O$ reconstructions based on $\delta^{18}O$ and Mg/Ca ratios in planktonic foraminifera. Four out of the six marine records from the Maritime Continent demonstrate especially strong coherence over the last millennium, characterized by a steady trend to more depleted (fresher/wetter) conditions from 1200 to 1700 CE, followed by a drying trend to present (Figure S3d). That this pattern is not shared by all marine records in this region is somewhat expected given the complexity of the surface ocean circulation in the Indonesian Archipelago. The inferred freshening across a broad sector of the Maritime Continent generally opposes the drying pattern in the South and East Asian records (to the north of the Maritime Continent) (Figure 3f) and also somewhat opposes the weak drying pattern in the single record from northern Australia (to the south of the Maritime Continent) (Figure S3c).

Notably, the reconstructed hydroclimate trends in the Maritime Continent are sensitive to the type of proxy archive (Figure S3); namely, this LIA signal is absent in many terrestrial records from the region, including two out of three lake sediment records (Figure S3e) and three out of three speleothem records (Figure S3f) from Indonesia and Borneo. These differences suggest that large-scale changes in moisture balance in the region may have been integrated into a regionally coherent seawater $\delta^{18}O$ signal, while terrestrial records reflect more localized precipitation changes and/or changes in moisture source and trajectories (e.g., Carolin et al., 2013). This interpretation is supported by the fact that there is considerable spatial heterogeneity in rainfall throughout the Indonesian archipelago, both in the annual mean and seasonal rainfall (As-syakur et al., 2013), which has been attributed to a complex interplay between the ocean, islands, topography, and the multitude of regional atmospheric circulation patterns in this region. Given this complexity, the marine reconstructions from the Maritime Continent offer a valuable set of additional hydroclimate constraints and provide robust evidence for coherent hydroclimate changes in this region during the LIA.

4.3.3. Dipole Pattern in South American Hydroclimate

The final piece of evidence that the LIA was marked by widespread changes in tropical hydroclimate comes from tropical South America, where the reconstructions show a distinct dipole pattern between the southwestern and northeastern sites between the LIA and MCA (Figure 4). Records from the central Andes and the southern Amazon generally indicate wet (and/or isotopically depleted) conditions from 1400 to 1700 CE, followed by a pronounced drying trend to the present (Figure 3e), while records from northern South America and Nordeste Brazil display a coherent drying (and/or isotopic enrichment) trend from 1300 to 1700 CE, followed by persistently dry conditions (Figure 3d). This dipole pattern is also apparent in the cluster analysis (Figures 2d–2g), the epoch analysis of the LIA versus MCA (Figure 4), and the EOF/PC analysis (Figure 6a).

Because all nine proxy records in the southwestern composite are water isotope records (Figure 3e), which integrate climate information over large spatial scales, the widespread signature of isotopic depletion in these records during the LIA is likely reflective of increased upstream rainout (either under enhanced SASM activity or increased rainfall in the monsoon entrance region), rather than changes in local rainfall amount (Vuille et al., 2012). The model results presented here do not support enhanced rainfall over the Amazon basin as the cause of the LIA isotopic depletion pattern in the central Andes and southern Amazon. Instead, they support upstream rainout in the monsoon entrance region in northeastern South America, as has also been found in isotope-enabled simulations with CESM (Orrison & Vuille, 2020).

Another possibility is that precipitation changes in tropical South America were caused by changes in tropical Pacific SSTs. However, if ENSO is the template, then the hydroclimate anomalies in northern South America and the Nordeste should be in phase with those in the central Andes, e.g., the warm phase of ENSO causes a drying in far northern South America and the Nordeste (Davey et al., 2014) as well as drying and isotopic enrichment in the central Andes and Amazon basin (Vuille & Werner, 2005), which is inconsistent with the proxy data.

An alternative explanation of the tropical South American records during the LIA is a southward shifted Atlantic ITCZ, as the ITCZ serves as the major conduit for moisture transport in the SASM region and responds sensitively to changes in the cross-equatorial SST gradient (Chiang, 2009; Chiang et al., 2002). There is ample evidence showing covariation in the Atlantic ITCZ and isotopic variations in the central Andes. For example, during the millennial-scale warm and cold events of the last ice age (i.e., Dansgaard-Oeschger oscillations) shifts of the Atlantic ITCZ, inferred from reflectance records from the Cariaco Basin (Deplazes et al., 2013), closely paralleled changes in the strength of the SASM (inferred from speleothem $\delta^{18}O$ records from the central Andes (Kanner et al., 2012)). However, the paleoclimate data from Nordeste Brazil are difficult to reconcile with the interpretation of a meridional shift of the Atlantic ITCZ during the LIA under northern tropical Atlantic cooling (Novello et al., 2012), as we would expect to see a strong antiphased relationship between the northern sites and Nordeste Brazil in response to a meridional shift of the ITCZ, when in fact we see the opposite.

A close in-phase relationship between hydroclimate records from the Cariaco Basin and Nordeste Brazil, such as observed over the last millennium, has also been documented from the last glacial period through the Holocene (Cruz et al., 2009; Novello et al., 2012). In those studies, the authors theorized that during

times of enhanced SASM activity, intense convection in the Amazon basin produces compensating large-scale subsidence in surrounding regions (more specifically, enhanced convective heating in the southwest Amazon intensifies the Bolivian High-Nordeste Low pressure system, which leads to increased subsidence and decreased summer precipitation over northeast Brazil) (Lenters & Cook, 1997; Novello et al., 2012).

We present a plausible alternative interpretation of the covariation between the northern South America and Nordeste Brazil records, namely that these records depict contractions and expansions of the Atlantic ITCZ, driven by coordinated changes in the northward and southward migrations of the Atlantic Ocean rain belt through the year. The Cariaco Basin sits beneath the northward extent of the western Atlantic ITCZ (Figure 1; Deplazes et al., 2013), while a substantial fraction of annual rainfall in Nordeste Brazil occurs when the Atlantic ITCZ is at its southernmost position between March and May (Novello et al., 2012), thus rainfall in these regions should be sensitive to changes in the northward and southward seasonal extremes of the ITCZ, respectively.

Indeed, recent modeling studies have indicated that the ocean rain bands expand and contract in response to changes in the interhemispheric temperature gradient under precessional forcing (Singarayer et al., 2017). The mechanism of the expansion/contraction in the models relates to the differential response of the hemispheres to insolation forcing. Since 1000 CE, insolation has decreased in boreal summer/fall when the Atlantic ITCZ is farthest north (Figure S2), and thus the ITCZ is not pulled as far away from the equator today compared to 1000 CE. In boreal winter/spring, when the ITCZ is farthest south, insolation has increased, and because it does so in both the northern and southern hemispheres, although the southern hemisphere warms, the northern hemisphere warms more because of the greater proportion of land there. Consequently, the boreal winter ITCZ shifts less far south in response. If these principles prevailed over the last millennium, as boreal summer/fall insolation decreased and boreal winter/spring insolation increased (Figure S2), the annual mean Atlantic ITCZ would be expected to contract, consistent with the drier conditions observed in both the Cariaco Basin and Nordeste Brazil (Figure 3d).

Additional support for this hypothesis is found in the early Holocene, when hydroclimate records indicate wetter conditions in the Cariaco Basin and Nordeste Brazil in the early Holocene relative to today (Cruz et al., 2009). During the early Holocene, boreal summer insolation was higher and boreal winter insolation was lower than present, and thus the boreal summer ITCZ would be expected to shift farther north and the boreal winter ITCZ would be expected to shift farther south, resulting in an expansion of the ITCZ, which is consistent with the wetter conditions recorded in both the Cariaco Basin and Nordeste Brazil during this time (Cruz et al., 2009). In model simulations, this behavior of the Atlantic ITCZ has been documented in time slice simulations of the last glacial cycle with the HadCM3 coupled climate model (Singarayer et al., 2017). In the present study, we see this behavior as a contraction of the Atlantic ITCZ over the last millennium in both the full forcing and orbital-only simulations with CESM (Figures 4, 5, and S4b), as well as in a number of the CMIP5/PMIP3 simulations (Figure S4a). The opposing seasonal rain band shifts are clear in the solstice seasons of all models, i.e., a northward shift in DJF and southward shift in JJA (see S6 for the ensemble means; individual models not shown), though they are more muted in the annual mean response of the CMIP5/PMIP3 models (Figure S4a).

While the simulated drying trend along the northern and southern edges of the Atlantic ITCZ does not extend over the South American continent in most models, the large spatial scale of this hydroclimate feature warrants serious consideration in interpreting the proxy reconstructions, particularly given the large uncertainties associated with the coarse spatial resolution and large tropical mean state biases in the models (PAGES Hydro2k Consortium, 2017). The clear covariation of paleo-hydroclimate records from northern South America and Nordeste Brazil over the precessional cycle and during the last millennium, in concert with the simulated contraction/expansion of the Atlantic ITCZ in response to precessional forcing in a diverse array of models, provides compelling evidence that a contraction of the Atlantic ITCZ is a plausible mechanism of the observed hydroclimate changes in northern South America and Nordeste Brazil over the last millennium. Notably, the central Andes and southern Amazon records more closely track the Asian monsoon records (with an antiphase relationship) than they do the records from northern South America and Nordeste Brazil, especially during the reversal of the LIA hydroclimate trends around 1600 CE, suggesting that the tropical Atlantic rain band evolved somewhat differently from rainfall in monsoon regions over the last millennium.

4.3.4. Correspondence Between the Tropical Hydroclimate and Temperature Changes

As discussed above, the period from 1400 to 1700 CE stands out as a time of pronounced tropical hydroclimate change across the tropics. These changes include drier (and/or isotopically enriched conditions) in South and East Asia, wetter (and/or isotopically depleted) conditions in the central Andes and southern Amazon, and fresher (and/or isotopically depleted) conditions in the Maritime Continent. Previous studies have highlighted the general correspondence between these hydroclimate changes and changes in the large-scale (global or northern hemisphere mean) temperature or changes in the interhemispheric temperature gradient (e.g., Sinha et al., 2011; Vuille et al., 2012; Yan et al., 2011). However, we find notable dissimilarities between the timing of these hydroclimate changes and the evolution of global mean temperature over the last millennium based on recent temperature reconstructions (Figure 3h; PAGES 2k Consortium, 2019). In particular, the hydroclimate composites from Asia (Figure 3f), southwestern South America (Figure 3e), and the Maritime Continent (Figure 3g) all indicate a reversal in the LIA hydroclimate trends around 1600–1700 CE (Figures 3e–3g, S12a, and S3d), while the reversal of global cooling occurs substantially later, around 1800 CE, in the ensemble median of the PAGES 2k Consortium (2019) temperature reconstructions (Figure 3h). There is substantial uncertainty across the statistical methods used to reconstruct global mean surface temperature, however, and one of the seven reconstruction methods (the Bayesian hierarchical model) indicates an early termination to the LIA around 1600–1700 CE, mirroring the pattern observed in the hydroclimate reconstructions.

In the proxy records, the reversal of the LIA hydroclimate trends around 1600–1700 CE is remarkably consistent across the regional composites of South and East Asia, South America, and the Maritime Continent, and is also reflected in Clusters 2 and 3 from the cluster analysis (Figures 2d and 2f). While the age model uncertainty in the reconstructions must be taken into account (particularly in the ^{14}C-dated marine and lake sediment records with few age control points; Table S1), the Asian and South American composites are dominated by well-dated speleothem records, and thus the synchronicity of this feature across a wide range of proxy archives from different regions of the tropics supports the inference of a widespread reversal in LIA hydroclimate trends around 1600–1700 CE.

The fact that Cluster 1 from the hydroclimate records tracks the reconstructed global temperature trends over the last millennium is consistent with our interpretation of this cluster as reflecting reduced evaporation rates under pan-tropical cooling (Falster et al., 2019). That the reconstructed *regional* hydroclimate anomalies do not track the global temperature trends is perhaps unsurprising, given that changes in tropical rainfall patterns would be expected to track the interhemispheric temperature gradient and/or regional temperature patterns more closely than global temperature trends. Recent reconstructions of the interhemispheric temperature gradient (Neukom et al., 2014) do indeed mirror the hydroclimate trends from 1400 CE to present, however the interhemispheric gradient diverges from the hydroclimate trends earlier in the millennium, e.g., during the temperature gradient minimum around 1200–1300 CE (Figure 3h). These discrepancies may reflect uncertainty in the reconstructions, or they may indicate that the regional hydroclimate anomalies during the LIA were not simply related to changes in the interhemispheric temperature gradient. Regardless, it is clear that more work needs to be done to understand the mechanisms of the widespread tropical hydroclimate changes around 1400–1700 CE. A targeted assessment of the regional temperature changes in the tropics over the last millennium would help better constrain the mechanisms.

4.4. Reevaluation of Tropical Pacific Climate Changes Over the Last Millennium

We now reexamine a number of longstanding hypotheses about the nature of tropical Pacific hydroclimate changes during the LIA. These hypotheses include: (a) a southward shift of the mean annual position of the Pacific ITCZ (Nelson & Sachs, 2016; Richey & Sachs, 2016; Sachs et al., 2009), (b) an equatorward contraction of the western Pacific and Asian-Australian rain band (Denniston et al., 2016; Griffiths et al., 2016; Yan et al., 2015), and (c) a strengthened Pacific Walker Circulation (Griffiths et al., 2016; Yan et al., 2011; Yan et al., 2015). We briefly evaluate the evidence for each and highlight the areas where additional corroboration is needed.

4.4.1. A Large-Scale Southward Shift of the Pacific ITCZ During the LIA?

A number of previous studies have postulated that a coordinated, large-scale southward shift of the ITCZ occurred during the relatively cool epoch of the LIA, arguing that this interpretation is consistent with dynamical theory that links the zonal mean ITCZ latitude to the interhemispheric energy budget and temperature gradient (Broecker & Putnam, 2013; Lechleitner et al., 2017; Nelson & Sachs, 2016; Richey & Sachs, 2016; Sachs et al., 2009). This theory has been invoked in the inference of a southward shift of both the Pacific rain band (Sachs et al., 2009) and Atlantic rain band (Haug et al., 2001) during the LIA.

We do not find broad support for a large-scale southward shift of the Pacific ITCZ during the LIA. First, no clear evidence of a large-scale southward shift in the Pacific rain band is observed when all available records from the central and eastern Pacific (where the Pacific ITCZ is well-defined) are compiled. While an abrupt transition to arid conditions around 1450 CE is clear in the Washington Island record from the central Pacific (Sachs et al., 2009; Figures 3a and S3b), given its location under the southern margin of the Pacific ITCZ in the present climate, dry conditions at that location would be more likely to be associated with a northerly shift of the Pacific ITCZ (Figure 1), as occurs in association with an enhanced Pacific Walker Circulation during La Niña events. Furthermore, there is also no synchronous shift in the eastern equatorial Pacific records around this time (Figure 3a), which lie just south of the southern extent of the eastern Pacific rain band (Figure 1), and thus would be expected to experience wetter conditions under a southward shift of the Pacific ITCZ. Second, the theoretical framework for a southward shift of the Pacific ITCZ during the LIA is lacking. Comprehensive climate models indicate that large-scale shifts in the tropical rain bands occur only under strong hemispheric asymmetry in radiative forcing, and even in those cases, the tropical Pacific rain band does not shift uniformly (e.g., Atwood et al., 2020). Ultimately, robust conclusions regarding changes in the Pacific ITCZ during the LIA will require more proxy data from the central and eastern Pacific, where the Pacific ITCZ is well-defined. Modern process studies would also help refine the interpretation of some existing records. For example, while all records from the Galápagos Islands demonstrate pronounced drying from 800–1000 CE, the records show less consistency in the latter part of the last millennium (Figure 3a) with the highland lake records (Atwood & Sachs, 2014; Conroy et al., 2008) agreeing with one another but showing distinct behavior from the coastal lake records (Nelson & Sachs, 2016). Ongoing efforts to develop additional hydroclimate reconstructions from the Galápagos Islands and calibrate proxy data against modern instrumental data should yield important insights in this data-sparse region of the tropical Pacific (e.g., Martin et al., 2018).

In summary, the evidence does not support a large-scale southward shift of the Pacific ITCZ during the LIA. As additional paleoclimate records are developed from the central and eastern tropical Pacific, all viable mechanisms of decadal rainfall variations in this region should be considered in the interpretation of the records, including changes in the width, intensity, and seasonal cycle of the Pacific rain band (Bartos et al., 2018; Byrne et al., 2018; Singarayer et al., 2017; Wodzicki & Rapp, 2016), as well as changes in the variability and spatial characteristics of the El Niño/Southern Oscillation.

4.4.2. Strengthened Pacific Walker Circulation During the LIA?

Other studies have compiled various hydroclimate records from the tropical Pacific and surrounding regions to infer a strengthened Pacific Walker Circulation during the LIA relative to the MCA (Griffiths et al., 2016; Yan et al., 2011; Yan et al., 2015). The marine records from the Maritime Continent indicating isotopically depleted (fresher) conditions during the LIA generally support this interpretation (Figure 3g), as does the Washington Island record in the central tropical Pacific, which indicates an abrupt shift to drier conditions around 1450 CE (Figures 3a and S3b). However, there is no evidence of drier conditions in the eastern equatorial Pacific in association with a strengthened Pacific Walker Circulation during the LIA (Figure 3a). This apparent discrepancy may be explained by the fact that the Galápagos Islands are situated in the already dry zone of the Pacific cold tongue and thus may experience little change in average rainfall under an enhanced Walker Circulation. The available data thus supports LIA freshening in parts of the Maritime Continent, with a possible linkage to central Pacific drying (based on a single record), but with no clear connection to the eastern Pacific. We therefore conclude that until further paleoclimate records are developed from the tropical Pacific, inferences of a strengthened Pacific Walker Circulation during the LIA remain speculative. Additional proxy sites near the Pacific rain bands could be especially helpful in this regard, as the rain bands

would be expected to expand poleward (equatorward) under an enhanced (weakened) Pacific Walker Circulation as occurs in association with the El Niño/Southern Oscillation (Wallace et al., 1998).

4.4.3. Contraction of the Monsoonal Asian-Australian Rain Belt During the LIA?

Another hypothesized large-scale reorganization in tropical climate during the LIA has been proposed based on proxy data from the western edge of the Pacific basin. Various compilations of records from the Maritime Continent, Australia, and East Asia have been interpreted as representing an equatorward contraction of rainfall at various periods within the LIA (ranging from 1400 to 1640 CE (Denniston et al., 2016), 1400 to 1850 CE (Yan et al., 2015), and 1500 to 1900 CE [Griffiths et al., 2016]). Our findings of drying in Asia and wetting in the Maritime Continent near the equator generally align with these prior studies, though there are some aspects of this interpretation that remain tenuous due to limited data availability. In particular, support for an equatorward contraction and/or weakening of the Australian monsoon during the LIA presented in Denniston et al. (2016) and Griffiths et al. (2016) rely on a single record from the Australian monsoon region (Denniston et al., 2016). Our analyses indicate that this record is consistent with a modest weakening of the Australian monsoon from 1400 to 1600 CE followed by a pronounced intensification to the modern era, though notably the LIA conditions are not anomalous with respect to background conditions of the Common Era (Figure S3c). Although eight records from the southern edge of the Australian Summer Monsoon were presented in the analysis of Yan et al. (2015), only three of these records spanned the last millennium, and of these, only one record (Denniston et al., 2016) was publicly available and thus used in our analysis. In addition, in the analyses presented in Yan et al. (2015), the reference period varied between the MCA and the last 150 years for different records in their compilation, depending on record length. We see large differences between the MCA and the last 200 years in many records in our analysis, and thus we strongly advocate for a standardized treatment across all proxy records in future studies so that the trends over the last few hundred years are separable from the changes between the MCA and LIA.

To robustly test the hypothesis of a coordinated contraction of the monsoonal Asian-Australian rain belt over the last millennium, additional records from the Australian monsoon region are needed. In addition, this hypothesis would benefit from a plausible set of physical mechanisms that could explain a coordinated response of the two highly seasonal and out-of-phase monsoonal rainfall regimes in Asia and Australia.

4.5. Insights From Data-Model Comparisons

Our primary objective in comparing the hydroclimate reconstructions to last millennium climate model simulations is to shed light on the possible mechanisms of the reconstructed hydroclimate changes. There are several ways in which the models lend important insight to the reconstructions. First, the fact that both proxies and models indicate drier conditions over South and East Asia during the second half of the last millennium provides evidence that the inferred weakening of the Asian monsoons during the LIA may have been forced in part by volcanic aerosols and/or orbital changes. However, the data-model mismatch in the timing of the drying trends over Asia (i.e., aridity peaks around 1600 CE in the reconstructions while the drying trend extends to at least 1800 CE in the models) indicates that there are clear deficiencies in the models' ability to capture this important feature of tropical hydroclimate change over the last millennium.

South America is another region where the models potentially provide new insight into the reconstructions. At first glance, tropical South America is seemingly characterized by pronounced data/model disagreement, as the simulated precipitation and the reconstructed hydroclimate changes are both robust but differ from one another in sign at the location of the proxy sites (Figure 4). The reconstructions show a distinct dipole pattern between the southwestern and northeastern sites between the LIA and MCA, which past studies have interpreted as reflecting increased upstream rainout under enhanced SASM activity during the LIA in tandem with subsidence and decreased summer precipitation over northeastern Brazil (Lenters & Cook, 1997; Novello et al., 2012; Vuille et al., 2012). In contrast, the models do not simulate an enhanced SASM during the LIA; however, they do simulate increased rainfall in the monsoon entrance region in the far northeastern corner of South America, that is driven by orbital and volcanic forcing. The simulations thus provide an alternative interpretation of the proxy data: that the observed LIA isotopic depletion in the central Andes and southern Amazon records reflects increased upstream rainout in the monsoon entrance region in northeastern South America (instead of enhanced SASM activity in the Amazon basin). If this

was indeed the case, however, the region of enhanced precipitation must have been confined to a narrow band near the equator, given the LIA drying (and/or isotopic enrichment) signal in both the northern and Nordeste records.

Also of relevance to the South American records, is the potential data-model agreement in the large-scale hydroclimate dynamics in the tropical Atlantic Ocean over the last millennium. A number of models simulate a contraction of the Atlantic ITCZ along one or both edges of the Atlantic rain band (Figures 4 and S4), while the reconstructions indicate a progressive shift to drier conditions along both the northward edge of the Atlantic ITCZ (Cariaco Basin and Columbian Andes) and the southward edge of the Atlantic ITCZ (Nordeste Brazil) (Figure 3d). To better assess the plausibility of these mechanisms in driving the observed hydroclimate signals in tropical South America, simulations with water isotope tracers should be included in future data-model comparison studies.

Finally, the models also potentially provide insight into the tropical Pacific climate reconstructions. The tropical Pacific proxy records are most closely aligned with individual CESM ensemble members that feature unforced centennial-scale changes in the strength of the Pacific Walker Circulation (Figure S8) and are also aligned with the CESM ensemble mean response that is characterized by a weak equatorial Pacific drying trend and wetting in the Maritime Continent west of Papua New Guinea (Figures 4c and 4d). Given the larger magnitude of internal variability relative to the forced response in CESM, and the fact that the pattern of internal variability projects onto the forced response in the regions of the tropical Pacific proxy data, these results suggest that, to the extent that CESM is representative of the real world, the observed tropical Pacific hydroclimate changes during the LIA are likely due to natural variations in the strength of the Walker Circulation. However, because the magnitude of tropical Pacific climate variability varies widely across models (and is largest in CESM where the variance of Niño 3 SST anomalies is around 150% of that observed over the last several decades), we caution that the model uncertainty precludes firm confidence in the interpretation of an unforced strengthening of the Pacific Walker Circulation during the LIA.

Outside of these potential areas of data-model agreement, one unresolved aspect of the reconstructed hydroclimate changes that is not reproduced by the models is the timing of widespread LIA hydroclimate changes in Asia, South America, and the Maritime Continent from 1400 to 1700 CE. There are several possible reasons for this data-model mismatch: (a) the reconstructed LIA hydroclimate changes were unforced, (b) the observed changes were forced but model uncertainty renders an unrealistic model response, (c) the observed changes were forced but uncertainty in the forcing renders an unrealistic model response, and/or (d) the proxy records, which are predominately derived from water isotope-based archives, reflect something other than changes in regional mean annual precipitation amount. We discuss each of these possibilities in more detail below.

With regard to (a), it is entirely possible that the reconstructed hydroclimate changes from 1400 to 1700 CE were produced by natural variability, although the broadly synchronous nature of the hydroclimate anomalies and hemispheric-scale temperature changes around this time is somewhat suggestive of a forced response in the climate system. However, with regards to (b), it is also expected that coupled ocean-atmosphere general circulation models would have difficulty reproducing the regional tropical hydroclimate response to last millennium forcings, given the highly parameterized nature of convection and cloud physics, and the limited ability of CMIP5 models to reproduce observed regional hydroclimate dynamics associated with major hydroclimate phenomena such as the Asian and North American monsoons (Flato, 2013; PAGES Hydro2k Consortium, 2017). Future data-model comparisons of the last millennium should address the ability of the models to simulate the first-order features of the key hydroclimate phenomena of interest. It has also been suggested that coupled climate models may underestimate the strength and persistence of the hydroclimate response to volcanic forcing (Tejedor et al., 2021), which if true, could severely limit the ability of such models to realistically capture the long-term hydroclimate responses to volcanic forcing over the last millennium. Finally, paleoclimate simulations do not typically include processes such as dynamic vegetation (which require ocean-atmosphere-vegetation general circulation models), although it is known that land surface processes are integral to the cycling of water between the land and atmosphere. Indeed, vegetation changes have been shown to reduce model-data discrepancies in simulations of the mid-Holocene (Braconnot et al., 2012).

With regards to (c), data-model discrepancies may result from errors in the radiative forcings and feedbacks. There are substantial uncertainties in the radiative forcings over the last millennium. For example, the radiative forcing during the LIA differs by more than a factor of 2 across the CMIP5/PMIP3 models due to differences in volcanic forcing (associated with both the aerosol data set used and the implementation method of the volcanic aerosols; see Section 2) (Atwood et al., 2016). These differences contribute to a factor of 2 spread in the amplitude of global cooling during the LIA across these models. These differences in volcanic forcing likely lead to differing tropical rainfall responses in the models, since tropical rainfall patterns are known to be sensitive to the timing, magnitude, and spatial footprint of volcanic eruptions (e.g., Colose et al., 2016; PAGES Hydro2k Consortium, 2017). Furthermore, because the volcanic aerosol loadings have changed (in both their magnitude and hemispheric distributions) in recently updated last millennium reconstructions (Figure S1; Sigl, McConnell, et al., 2014; Sigl, Winstrup, et al., 2015; Toohey & Sigl, 2017), the next iteration of model simulations may be expected to differ in their representation of volcanically forced tropical precipitation changes over the last millennium. In addition to the uncertainties in radiative forcing, there are also uncertainties in the strength and pattern of climate feedbacks among models. For example, the total effective feedback parameter during the LIA differs by a factor of 2 across the CMIP5/PMIP3 models (ranging from -1.0 to -2.0 W/m^2/K), largely due to differences in the shortwave cloud feedback, the lapse rate feedback, and the surface albedo feedback (Atwood et al., 2016). The degree of interhemispheric asymmetry in the feedback strengths also varies across models (Figure S13). Errors in the interhemispheric asymmetry of the forcings and feedbacks over the last millennium would be expected to lead to erroneous interhemispheric temperature asymmetry in the models. Indeed, the models, which reasonably reproduce the long-term global cooling trends in reconstructions, tend to substantially underestimate changes in the interhemispheric temperature asymmetry over the last millennium (Neukom et al., 2014). Given the evidence that the tropical hydroclimate anomalies may have been linked to the interhemispheric temperature gradient during the LIA, future data-model comparison efforts should target simulations that reasonably capture the interhemispheric temperature asymmetry during the LIA.

Finally, with regards to (d), it is likely that the proxy records used in this analysis, many of which are derived from water isotope-based archives, do not solely reflect changes in regional mean annual precipitation amount. The stable isotopic composition of meteoric water integrates information about many other aspects of the water cycle over space and time, including the seasonality of precipitation, sources of moisture, advective transport, evaporation, and water recycling over land. It is clear that more work needs to be done to understand the mechanisms of the widespread tropical hydroclimate changes around 1400–1700 CE. Future work should therefore employ climate models that simulate water isotope tracers and incorporate proxy system models to provide more quantitative comparisons between proxy reconstructions and model simulations of the last millennium.

5. Conclusions

We review the evidence for large-scale tropical hydroclimate changes over the Common Era based on a compilation of 67 tropical hydroclimate records and assess the consistency between the reconstructed hydroclimate changes and those simulated by forced transient model simulations of the last millennium. A hierarchal cluster analysis indicates that 41% of the records, distributed throughout the tropics, demonstrate a millennial-scale isotopic depletion/wetting trend beginning around 1000 CE and reversing around 1800 CE that generally tracks global temperature trends over the last millennium, which we speculate is associated with the influence of decreased tropical sea surface temperatures on the isotopic composition of water vapor.

Our synthesis of the proxy records also reveals a number of regionally coherent hydroclimate patterns. During the onset of the MCA around 800–1000 CE, records from the eastern equatorial Pacific and Mesoamerica indicate a pronounced drying event, relative to background conditions of the Common Era. The second half of the last millennium is characterized by a set of pronounced and synchronous hydroclimate changes across the tropics from 1400 to 1700 CE, including drier (isotopically enriched) conditions in South and East Asia, fresher (isotopically depleted) surface ocean conditions in the Maritime Continent, and a dipole pattern in tropical South America, with wet (isotopically depleted) conditions in the southwest and dry (isotopically enriched) conditions in northern South America and Nordeste Brazil. While previous studies

have linked these hydroclimate changes to global or hemispheric-scale cooling patterns, we find notable dissimilarities between the regional hydroclimate changes and global-scale and hemispheric-scale temperature reconstructions, indicating that more work needs to be done to understand the mechanisms of the widespread tropical hydroclimate changes during the LIA.

Considering previous interpretations of tropical Pacific climate change during the LIA, we do not find support for a large-scale southward shift of the Pacific ITCZ. We find that the available data generally support a strengthened the Pacific Walker Circulation during the LIA, with freshening in parts of the Maritime Continent, and a possible linkage to central Pacific drying (based on a single lake sediment record), but with no clear connection to the eastern Pacific. We therefore conclude that until further paleoclimate records are developed from the tropical Pacific, inferences of a strengthened Pacific Walker Circulation during the LIA remain speculative. Regarding the evidence for an equatorward contraction of the monsoonal Asian-Australian rain belt during the LIA, we caution that more work needs to be done to characterize the hydroclimate changes in the Australian monsoon region.

Lastly, transient climate model simulations of the last millennium provide several important insights to the interpretation of the reconstructions: (a) the observed drying and/or isotopic enrichment in South and East Asia during the LIA may reflect weakened summer monsoon activity driven in part by volcanic and orbital forcing, (b) the observed LIA isotopic depletion in the central Andes and southern Amazon may reflect upstream rainout in the SASM monsoon entrance region driven by orbital and volcanic forcing (rather than a strengthening of the monsoon), (c) the observed coordinated drying in northern South America and Nordeste Brazil over the last millennium may reflect a contraction of the Atlantic ITCZ, and (d) isotopically depleted conditions in the Maritime Continent during the LIA are consistent with a strengthening of the Pacific Walker Circulation, though the large model uncertainty in the tropical Pacific precludes confidence in this interpretation. One aspect of the reconstructed hydroclimate changes that remains unresolved is the mechanism of the LIA hydroclimate changes in Asia, South America, and the Maritime Continent from 1400 to 1700 CE, followed by a reversal of the LIA conditions to the present era. To better assess the mechanisms of the reconstructed LIA hydroclimate changes, future work should employ climate models that reasonably simulate tropical climate variability, represent the key hydroclimate phenomena of interest with reasonable accuracy, and explicity track water isotope ratios in the hydrosphere to improve comparisons between proxy reconstructions and model simulations of the last millennium.

Acknowledgments
The authors gratefully acknowledge all of the researchers who made their paleoclimate data available for public access and who participated in the CMIP5/PMIP3 and CESM LME modeling efforts and made the model output publicly available. Computing resources (https://doi.org/10.5065/D6RX99HX) were provided by the Climate Simulation Laboratory at NCAR's Computational and Information Systems Laboratory, sponsored by the National Science Foundation and other agencies. The output from the CMIP5/PMIP3 and CESM LME simulations was obtained from the Earth System Grid (earthsystemgrid.org). Support for this work was provided to ARA by the U.S. National Science Foundation under award AGS-1949605 and by the NSF Graduate Research Fellowship Program (DGE-1256082) and the NOAA Climate and Global Change Postdoctoral Program (under fellowships to ARA). Support was provided to EW and DMWF by NSF Awards AGS-0846641, AGS-0936059, AGS-1359464, and AGS-1665247. Support was provided to D. S. Battisti by the Tamaki Foundation, and to J. P. Sachs by NSF under Grant Nos. 0823503 and 1502417. The authors thank K. Shell for providing the CAM3 radiative kernels.

Data Availability Statement

The proxy data used in this study were uploaded to Figshare (https://figshare.com/articles/Hydroclimate_proxy_records_zip/12085092) and published with https://doi.org/10.6084/m9.figshare.12085092. The records were originally downloaded from the NOAA Paleoclimatology and PANGAEA databases (see data set URLs in Table 1), or obtained directly from the authors (see references in Table 1).

References

Anderson, D. M., Overpeck, J. T., & Gupta, A. K. (2002). Increase in the Asian southwest monsoon during the past four centuries. *Science*, *297*, 596–599. https://doi.org/10.1126/science.1072881

Apaéstegui, J., Cruz, F. W., Sifeddine, A., Vuille, M., Espinoza, J. C., Guyot, J. L., et al. (2014). Hydroclimate variability of the northwestern Amazon Basin near the Andean foothills of Peru related to the South American Monsoon System during the last 1600 years. *Climate of the Past*, *10*, 1967–1981. https://doi.org/10.5194/cp-10-1967-2014

As-syakur, A. R., Tanaka, T., Osawa, T., & Mahendra, M. S. (2013). Indonesian rainfall variability observation using TRMM multi-satellite data. *International Journal of Remote Sensing*, *34*, 7723–7738. https://doi.org/10.1080/01431161.2013.826837

Atwood, A. R., Donohoe, A., Battisti, D. S., Liu, X., & Pausata, F. S. R. (2020). Robust longitudinally-variable responses of the ITCZ to a myriad of climate forcings. *Geophysical Research Letters*, *47*, e2020GL088833. https://doi.org/10.1029/2020GL088833

Atwood, A. R., & Sachs, J. P. (2014). Separating ITCZ- and ENSO-related rainfall changes in the Galápagos over the last 3 kyr using D/H ratios of multiple lipid biomarkers. *Earth and Planetary Science Letters*, *404*, 408–419. https://doi.org/10.1016/j.epsl.2014.07.038

Atwood, A. R., Wu, E., Frierson, D. M. W., Battisti, D. S., & Sachs, J. P. (2016). Quantifying climate forcings and feedbacks over the last millennium in the CMIP5-PMIP3 models. *Journal of Climate*, *29*, 1161–1178. https://doi.org/10.1175/jcli-d-15-0063.1

Bartos, E. A., Rapp, A. D., & Wodzicki, K. R. (2018). Increasing frequency of midtropospheric dry layers in the pacific intertropical convergence zone. *Geophysical Research Letters*, *45*, 13523–13529. https://doi.org/10.1029/2018GL080799

Berkelhammer, M., Sinha, A., Mudelsee, M., Cheng, H., Edwards, R. L., & Cannariato, K. (2010). Persistent multidecadal power of the Indian Summer Monsoon. *Earth and Planetary Science Letters*, *290*, 166–172. https://doi.org/10.1016/j.epsl.2009.12.017

Bhattacharya, T., Byrne, R., Bohnel, H., Wogau, K., Kienelc, U., Ingram, B. L., & Zimmerman, S. (2015). Cultural implications of late Holocene climate change in the Cuenca Oriental, Mexico. *Proceedings of the National Academy of Sciences of the United States of America*, *112*, 1693–1698. https://doi.org/10.1073/pnas.1405653112

Bhattacharya, T., Chiang, J. C. H., & Cheng, W. (2017). Ocean-atmosphere dynamics linked to 800–1050 CE drying in mesoamerica. *Quaternary Science Reviews*, *169*, 263–277. https://doi.org/10.1016/j.quascirev.2017.06.005

Biasutti, M., Voigt, A., Boos, W. R., Braconnot, P., Hargreaves, J. C., Harrison, S. P., et al. (2018). Global energetics and local physics as drivers of past, present and future monsoons. *Nature Geoscience*, *11*, 392–400. https://doi.org/10.1038/s41561-018-0137-1

Bird, B. W., Abbott, M. B., Vuille, M., Rodbell, D. T., Stansell, N. D., & Rosenmeier, M. F. (2011). A 2,300-year-long annually resolved record of the South American summer monsoon from the Peruvian Andes. *Proceedings of the National Academy of Sciences of the United States of America*, *108*, 8583–8588. https://doi.org/10.1073/pnas.1003719108

Bird, B. W., Rudloff, O., Escobar, J., Gilhooly, W. P., Correa-Metrio, A., Vélez, M., & Polissar, P. J. (2017). Paleoclimate support for a persistent dry island effect in the Colombian Andes during the last 4700 years. *The Holocene*, *28*, 217–228. https://doi.org/10.1177/0959683617721324

Braconnot, P., Harrison, S. P., Kageyama, M., Bartlein, P. J., Masson-Delmotte, V., Abe-Ouchi, A., et al. (2012). Evaluation of climate models using palaeoclimatic data. *Nature Climate Change*, *2*, 417–424. https://doi.org/10.1038/nclimate1456

Breukelen, van, M. R., Vonhof, H. B., Hellstrom, J. C., Wester, W. C. G., & Kroon, D. (2008). Fossil dripwater in stalagmites reveals Holocene temperature and rainfall variation in Amazonia. *Earth and Planetary Science Letters*, *275*, 54–60. https://doi.org/10.1016/j.epsl.2008.07.060

Broecker, W. S., & Putnam, A. E. (2013). Hydrologic impacts of past shifts of Earth's thermal equator offer insight into those to be produced by fossil fuel CO_2. *Proceedings of the National Academy of Sciences of the United States of America*, *110*, 16710–16715. https://doi.org/10.1073/pnas.1301855110

Buckley, B. M., Anchukaitis, K. J., Penny, D., Fletcher, R., Cook, E. R., Sano, M., et al. (2010). Climate as a contributing factor in the demise of Angkor, Cambodia. *Proceedings of the National Academy of Sciences of the United States of America*, *107*, 6748–6752. https://doi.org/10.1073/pnas.0910827107

Byrne, M. P., Pendergrass, A. G., Rapp, A. D., & Wodzicki, K. R. (2018). Response of the intertropical convergence zone to climate change: Location, width, and strength. *Current Climate Change Reports*, *4*, 355–370. https://doi.org/10.1007/s40641-018-0110-5

Cai, Y., Tan, L., Cheng, H., An, Z., Edwards, R. L., Kelly, M. J., et al. (2010). The variation of summer monsoon precipitation in central China since the last deglaciation. *Earth and Planetary Science Letters*, *291*, 21–31. https://doi.org/10.1016/j.epsl.2009.12.039

Carolin, S. A., Cobb, K. M., Adkins, J. F., Clark, B., Conroy, J. L., Lejau, S., et al. (2013). Varied response of western pacific hydrology to climate forcings over the last glacial period. *Science*, *340*, 1564–1566. https://doi.org/10.1126/science.1233797

Carolin, S. A., Cobb, K. M., Lynch-Stieglitz, J., Moerman, J. W., Partin, J. W., Lejau, S., et al. (2016). Northern Borneo stalagmite records reveal West Pacific hydroclimate across MIS 5 and 6. *Earth and Planetary Science Letters*, *439*, 182–193. https://doi.org/10.1016/j.epsl.2016.01.028

Cheng, H., Sinha, A., Cruz, F. W., Wang, X., Edwards, R. L., d'Horta, F. M., et al. (2013). Climate change patterns in Amazonia and biodiversity. *Nature Communications*, *4*, 1411. https://doi.org/10.1038/ncomms2415

Chen, S., Hoffmann, S. S., Lund, D. C., Cobb, K. M., & Emile-Geay, J. (2016). A high-resolution speleothem record of western equatorial Pacific rainfall: Implications for Holocene ENSO evolution. *Earth and Planetary Science Letters*, *442*, 61–71. https://doi.org/10.1016/j.epsl.2016.02.050

Chiang, J. C. H. (2009). The tropics in paleoclimate. *Annual Review of Earth and Planetary Sciences*, *37*, 263–297. https://doi.org/10.1146/annurev.earth.031208.100217

Chiang, J. C. H., & Bitz, C. M. (2005). Influence of high latitude ice cover on the marine intertropical convergence zone. *Climate Dynamics*, *25*, 477–496. https://doi.org/10.1007/s00382-005-0040-5

Chiang, J. C. H., Kushnir, Y., & Giannini, A. (2002). Deconstructing Atlantic intertropical convergence zone variability: Influence of the local cross-equatorial sea surface temperature gradient and remote forcing from the eastern equatorial Pacific. *Journal of Geophysical Research*, *107*(D1), 4004. https://doi.org/10.1029/2000JD000307

Collins, M., Tett, S. F. B., & Cooper, C. (2001). The internal climate variability of HadCM3, a version of the Hadley Centre coupled model without flux adjustments. *Climate Dynamics*, *17*, 61–81. https://doi.org/10.1007/s003820000094

Colose, C. M., LeGrande, A. N., & Vuille, M. (2016). Hemispherically asymmetric volcanic forcing of tropical hydroclimate during the last millennium. *Earth System Dynamics*, *7*, 681–696. https://doi.org/10.5194/esd-7-681-2016

Conroy, J. L., Overpeck, J. T., Cole, J. E., Shanahan, T. M., & Steinitz-Kannan, M. (2008). Holocene changes in eastern tropical Pacific climate inferred from a Galápagos lake sediment record. *Quaternary Science Reviews*, *27*, 1166–1180. https://doi.org/10.1016/j.quascirev.2008.02.015

Crausbay, S. D., Russell, J. M., & Schnurrenberger, D. W. (2006). A ca. 800-year lithologic record of drought from sub-annually laminated lake sediment, East Java. *Journal of Paleolimnology*, *35*, 641–659. https://doi.org/10.1007/s10933-005-4440-7

Crowley, T. J., Zielinski, G., Vinther, B., Udisti, R., Kreutz, K., Cole-Dai, J., & Castellano, E. (2008). Volcanism and the Little Ice Age. *PAGES Newsletter*, *16*, 22–23. https://doi.org/10.22498/pages.16.2.22

Crucifix, M. (2006). Does the last glacial maximum constrain climate sensitivity? *Geophysical Research Letters*, *33*, L18701. https://doi.org/10.1029/2006GL027137

Cruz, F. W., Vuille, M., Burns, S. J., Wang, X., Cheng, H., Werner, M., et al. (2009). Orbitally driven east-west antiphasing of South American precipitation. *Nature Geoscience*, *2*, 210–214. https://doi.org/10.1038/ngeo444

Cunningham, L. K., Austin, W. E., Knudsen, K. L., Eiríksson, J., Scourse, J. D., Wanamaker, A. D., et al. (2013). Reconstructions of surface ocean conditions from the northeast Atlantic and Nordic seas during the last millennium. *The Holocene*, *23*, 921–935. https://doi.org/10.1177/0959683613479677

Curtis, J. H., Brenner, M., Hodell, D. A., Balser, R. A., Islebe, G. A., & Hooghiemstra, H. (1998). A multi-proxy study of Holocene environmental change in the Maya Lowlands of Peten, Guatemala. *Journal of Paleolimnology*, *19*, 139–159.

Curtis, J. H., Hodell, D. A., & Brenner, M. (1996). Climate variability on the Yucatan Peninsula (Mexico) during the past 3500 years, and implications for Maya cultural evolution. *Quaternary Research*, *46*, 37–47.

Dansgaard, W. (1964). Stable isotopes in precipitation. *Tellus*, *16*, 436–468. https://doi.org/10.3402/tellusa.v16i4.8993

Davey, M. K., Brookshaw, A., & Ineson, S. (2014). The probability of the impact of ENSO on precipitation and near-surface temperature. *Climate Risk Management*, *1*, 5–24. https://doi.org/10.1016/j.crm.2013.12.002

Denniston, R. F., Ummenhofer, C. C., Wanamaker, A. D., Lachniet, M. S., Villarini, G., Asmerom, Y., et al. (2016). Expansion and contraction of the indo-pacific tropical rain belt over the last three millennia. *Scientific Reports*, *6*, 34485. https://doi.org/10.1038/srep34485

Deplazes, G., Lückge, A., Peterson, L. C., Timmermann, A., Hamann, Y., Hughen, K. A., et al. (2013). Links between tropical rainfall and North Atlantic climate during the last glacial period. *Nature Geoscience*, *6*, 213–217. https://doi.org/10.1038/ngeo1712

Dong, J., Wang, Y., Cheng, H., Hardt, B., Edwards, R. L., Kong, X., et al. (2010). A high-resolution stalagmite record of the Holocene East Asian monsoon from Mt Shennongjia, central China. *The Holocene*, *20*, 257–264. https://doi.org/10.1177/0959683609350393

Donohoe, A., Marshall, J., Ferreira, D., & McGee, D. (2013). The relationship between ITCZ location and cross-equatorial atmospheric heat transport: From the seasonal cycle to the last glacial maximum. *Journal of Climate*, *26*, 3597–3618. https://doi.org/10.1175/jcli-d-12-00467.1

Dykoski, C. A., Edwards, R. L., Cheng, H., Yuan, D., Cai, Y., Zhang, M., et al. (2005). A high-resolution, absolute-dated Holocene and deglacial Asian monsoon record from Dongge Cave, China. *Earth and Planetary Science Letters*, *233*, 71–86. https://doi.org/10.1016/j.epsl.2005.01.036

Eisen, M. B., Spellman, P. T., Brown, P. O., & Botstein, D. (1998). Cluster analysis and display of genome-wide expression patterns. *Proceedings of the National Academy of Sciences of the United States of America*, *95*, 14863–14868. https://doi.org/10.1073/pnas.95.25.14863

Emile-Geay, J., McKay, N. P., Kaufman, D. S., Gunten, von, L., Wang, J., Anchukaitis, K. J., et al. (2017). A global multiproxy database for temperature reconstructions of the Common Era. *Scientific Data*, *4*, 170088.

Escobar, J., Hodell, D. A., Brenner, M., Curtis, J. H., Gilli, A., Mueller, A. D., et al. (2012). A ~43-ka record of paleoenvironmental change in the Central American lowlands inferred from stable isotopes of lacustrine ostracods. *Quaternary Science Reviews*, *37*, 92–104. https://doi.org/10.1016/j.quascirev.2012.01.020

Falster, G., Konecky, B. L., McKay, N., Atwood, A. R., Conroy, J. L., Fischer, M., et al. (2019). New insights into spatial and temporal dynamics of the global water cycle from the Iso2k database. AGU Fall Meeting.

Fernández-Donado, L., González-Rouco, J. F., Raible, C. C., Ammann, C. M., Barriopedro, D., García-Bustamante, E., et al. (2013). Large-scale temperature response to external forcing in simulations and reconstructions of the last millennium. *Climate of the Past*, *9*, 393–421. https://doi.org/10.5194/cp-9-393-2013

Flato, G., Marotzke, J., Abiodun, B., Braconnot, P., Chou, S. C., Collins, W., et al. (2013). Evaluation of climate models. In T. F. Stocker, D. Qin, G.-K. Plattner, M. Tignor, S. K. Allen, J. Boschung, et al. (Eds.), *Climate change 2013: The physical science basis. Contribution of working group I to the fifth assessment report of the intergovernmental panel on climate change*. Cambridge University Press.

Gao, C., Robock, A., & Ammann, C. (2008). Volcanic forcing of climate over the past 1500 years: An improved ice core-based index for climate models. *Journal of Geophysical Research: Atmospheres*, *113*, D231111. https://doi.org/10.1029/2008JD010239

Gent, P. R., Danabasoglu, G., Donner, L. J., Holland, M. M., Hunke, E. C., Jayne, S. R., et al. (2011). The community climate system model version 4. *Journal of Climate*, *24*, 4973–4991. https://doi.org/10.1175/2011jcli4083.1

Griffiths, M. L., Drysdale, R. N., Gagan, M. K., Zhao, J.-X., Ayliffe, L. K., Hellstrom, J. C., et al. (2009). Increasing Australian–Indonesian monsoon rainfall linked to early Holocene sea-level rise. *Nature Geoscience*, *2*, 636–639. https://doi.org/10.1038/NGEO605

Griffiths, M. L., Kimbrough, A. K., Gagan, M. K., Drysdale, R. N., Cole, J. E., Johnson, K. R., et al. (2016). Western Pacific hydroclimate linked to global climate variability over the past two millennia. *Nature Communications*, *7*, 11719. https://doi.org/10.1038/ncomms11719

Haug, G. H., Hughen, K. A., Sigman, D. M., Peterson, L. C., & Rohl, U. (2001). Southward migration of the intertropical convergence zone through the Holocene. *Science*, *293*, 1304–1308. https://doi.org/10.1126/science.1059725

Hegerl, G. C., Crowley, T. J., Allen, M., Hyde, W. T., Pollack, H. N., Smerdon, J., & Zorita, E. (2007). Detection of human influence on a new, validated 1500-year temperature reconstruction. *Journal of Climate*, *20*, 650–666. https://doi.org/10.1175/jcli4011.1

Higley, M. C., Conroy, J. L., & Schmitt, S. (2018). Last millennium meridional shifts in hydroclimate in the central tropical Pacific. *Paleoceanography and Paleoclimatology*, *33*, 354–366. https://doi.org/10.1002/2017PA003233

Hillman, A. L., Yu, J., Abbott, M. B., Cooke, C. A., Bain, D. J., & Steinman, B. A. (2014). Rapid environmental change during dynastic transitions in Yunnan Province, China. *Quaternary Science Reviews*, *98*, 24–32. https://doi.org/10.1016/j.quascirev.2014.05.019

Hodell, D. A., Anselmetti, F. S., Ariztegui, D., Brenner, M., Curtis, J. H., Gilli, A., et al. (2008). An 85-ka record of climate change in lowland Central America. *Quaternary Science Reviews*, *27*, 1152–1165. https://doi.org/10.1016/j.quascirev.2008.02.008

Hodell, D. A., Brenner, M., & Curtis, J. H. (2005). Terminal classic drought in the northern Maya lowlands inferred from multiple sediment cores in Lake Chichancanab (Mexico). *Quaternary Science Reviews*, *24*, 1413–1427. https://doi.org/10.1016/j.quascirev.2004.10.013

Hu, C., Henderson, G. M., Huang, J., Xie, S., Sun, Y., & Johnson, K. R. (2008). Quantification of Holocene Asian monsoon rainfall from spatially separated cave records. *Earth and Planetary Science Letters*, *266*, 221–232. https://doi.org/10.1016/j.epsl.2007.10.015

Hwang, Y. T., Frierson, D. M. W., & Kang, S. M. (2013). Anthropogenic sulfate aerosol and the southward shift of tropical precipitation in the late 20th century. *Geophysical Research Letters*, *40*, 2845–2850. https://doi.org/10.1002/grl.50502

Kang, S. M., Held, I. M., Frierson, D. M. W., & Zhao, M. (2008). The response of the ITCZ to extratropical thermal forcing: Idealized slab-ocean experiments with a GCM. *Journal of Climate*, *21*, 3521–3532. https://doi.org/10.1175/2007jcli2146.1

Kanner, L. C., Burns, S. J., Cheng, H., & Edwards, R. L. (2012). High-latitude forcing of the South American summer monsoon during the last glacial. *Science*, *335*, 570–573. https://doi.org/10.1126/science.1213397

Kanner, L. C., Burns, S. J., Cheng, H., Edwards, R. L., & Vuille, M. (2013). High-resolution variability of the South American summer monsoon over the last seven millennia: Insights from a speleothem record from the central Peruvian Andes. *Quaternary Science Reviews*, *75*, 1–10. https://doi.org/10.1016/j.quascirev.2013.05.008

Kaufman, D. S., Axford, Y. L., Henderson, A. C. G., McKay, N. P., Oswald, W. W., Saenger, C., et al. (2016). Holocene climate changes in eastern Beringia (NW North America)—A systematic review of multi-proxy evidence. *Quaternary Science Reviews*, *147*, 312–339. https://doi.org/10.1016/j.quascirev.2015.10.021

Kaufman, D. S., Schneider, D. P., McKay, N. P., Ammann, C. M., Bradley, R. S., Briffa, K. R., et al. (2009). Recent warming reverses long-term arctic cooling. *Science*, *325*, 1236–1239. https://doi.org/10.1126/science.1173983

Kobashi, T., Kawamura, K., Severinghaus, J. P., Barnola, J.-M., Nakaegawa, T., Vinther, B. M., et al. (2011). High variability of Greenland surface temperature over the past 4000 years estimated from trapped air in an ice core. *Geophysical Research Letters*, *38*, L21501. https://doi.org/10.1029/2011GL049444

Konecky, B. L., McKay, N. P., Churakova, O. V., Comas-Bru, L., Dassié, E. P., DeLong, K. L., et al. (2020). The Iso2k database: A global compilation of paleo-$\delta^{18}O$ and $\delta^{2}H$ records to aid understanding of Common Era climate. *Earth System Science Data Discussions*, *12*, 2261–2288. https://doi.org/10.5194/essd-12-2261-2020

Konecky, B. L., Russell, J. M., Rodysill, J. R., Vuille, M., Bijaksana, S., & Huang, Y. (2013). Intensification of southwestern Indonesian rainfall over the past millennium. *Geophysical Research Letters*, *40*, 386–391. https://doi.org/10.1029/2012GL054331

Lachniet, M. S., Bernal, J. P., Asmerom, Y., Polyak, V., & Piperno, D. (2012). A 2400 yr Mesoamerican rainfall reconstruction links climate and cultural change. *Geology*, *40*, 259–262. https://doi.org/10.1130/g32471.1

Landrum, L., Otto-Bliesner, B. L., Wahl, E. R., Conley, A., Lawrence, P. J., Rosenbloom, N., & Teng, H. (2013). Last millennium climate and its variability in CCSM4. *Journal of Climate*, *26*, 1085–1111. https://doi.org/10.1175/jcli-d-11-00326.1

Lechleitner, F. A., Breitenbach, S. F. M., Rehfeld, K., Ridley, H. E., Asmerom, Y., Prufer, K. M., et al. (2017). Tropical rainfall over the last two millennia: Evidence for a low-latitude hydrologic seesaw. *Scientific Reports*, *7*, 45809.

Lehner, F., Born, A., Raible, C. C., & Stocker, T. F. (2013). Amplified inception of European little ice age by sea ice-ocean-atmosphere feedbacks. *Journal of Climate*, *26*, 7586–7602. https://doi.org/10.1175/jcli-d-12-00690.1

Lenters, J. D., & Cook, K. H. (1997). On the origin of the Bolivian high and related circulation features of the South American climate. *Journal of the Atmospheric Sciences*, *54*, 656–678. https://doi.org/10.1175/1520-0469(1997)054<0656:otootb>2.0.co;2

Maloney, A. (2018). *Tropical South Pacific paleohydrology from hydrogen isotopes in algal lipids* (PhD dissertation). University of Washington.

Mann, M. E., Zhang, Z., Rutherford, S., Bradley, R. S., Hughes, M. K., Shindell, D., et al. (2009). Global signatures and dynamical origins of the little ice age and medieval climate anomaly. *Science*, *326*, 1256–1260. https://doi.org/10.1126/science.1177303

Marcott, S. A., Shakun, J. D., Clark, P. U., & Mix, A. C. (2013). A reconstruction of regional and global temperature for the past 11,300 years. *Science*, *339*, 1198–1201. https://doi.org/10.1126/science.1228026

Marsland, S. J., Haak, H., Jungclaus, J. H., Latif, M., & Röske, F. (2003). The Max-Planck-Institute global ocean/sea ice model with orthogonal curvilinear coordinates. *Ocean Modelling*, *5*, 91–127. https://doi.org/10.1016/s1463-5003(02)00015-x

Martin, N. J., Conroy, J. L., Noone, D., Cobb, K. M., Konecky, B. L., & Rea, S. (2018). Seasonal and ENSO influences on the stable isotopic composition of Galápagos precipitation. *Journal of Geophysical Research: Atmospheres*, *123*, 261–275. https://doi.org/10.1002/2017JD027380

Masse, G., Rowland, S. J., Sicre, M. A., Jacob, J., Jansen, E., & Belt, S. T. (2008). Abrupt climate changes for Iceland during the last millennium: Evidence from high resolution sea ice reconstructions. *Earth and Planetary Science Letters*, *269*, 564–568. https://doi.org/10.1016/j.epsl.2008.03.017

Masson-Delmotte, V., Schulz, M., Abe-Ouchi, A., Beer, J., Ganopolski, A., González Rouco, J. F., et al. (2013). Information from Paleoclimate Archives. In T. F. Stocker, D. Qin, G.-K. Plattner, M. Tignor, S. K. Allen, J. Boschung, et al. (Eds.), Climate change 2013: The physical science basis. Contribution of working group I to the fifth assessment report of the intergovernmental panel on climate change. Cambridge University Press.

Medina-Elizalde, M., Burns, S. J., Lea, D. W., Asmerom, Y., Gunten, von, L., Polyak, V., et al. (2010). High resolution stalagmite climate record from the Yucatán Peninsula spanning the Maya terminal classic period. *Earth and Planetary Science Letters*, *298*, 255–262. https://doi.org/10.1016/j.epsl.2010.08.016

Metcalfe, S. E., Jones, M. D., Davies, S. J., Noren, A., & MacKenzie, A. (2010). Climate variability over the last two millennia in the North American Monsoon region, recorded in laminated lake sediments from Laguna de Juanacatlán, Mexico. *The Holocene*, *20*, 1195–1206. https://doi.org/10.1177/0959683610371994

Moberg, A., Sonechkin, D. M., Holmgren, K., Datsenko, N. M., & Karlén, W. (2005). Highly variable Northern Hemisphere temperatures reconstructed from low- and high-resolution proxy data. *Nature*, *433*, 613–617. https://doi.org/10.1038/nature03265

Moy, C. M., Seltzer, G. O., Rodbell, D. T., & Anderson, D. M. (2002). Variability of El Nino/Southern Oscillation activity at millennial timescales during the Holocene epoch. *Nature*, *420*, 162–165. https://doi.org/10.1038/nature01194

Nelson, D. B., & Sachs, J. P. (2016). Galápagos hydroclimate of the Common Era from paired microalgal and mangrove biomarker $^{2}H/^{1}H$ values. *Proceedings of the National Academy of Sciences of the United States of America*, *113*, 3476–3481. https://doi.org/10.1073/pnas.1516271113

Neukom, R., Gergis, J., Karoly, D. J., Wanner, H., Curran, M., Elbert, J., et al. (2014). Inter-hemispheric temperature variability over the past millennium. *Nature Climate Change*, *4*, 362–367. https://doi.org/10.1038/nclimate2174

Newton, A., Thunell, R., & Stott, L. (2006). Climate and hydrographic variability in the Indo-Pacific Warm Pool during the last millennium. *Geophysical Research Letters*, *33*, L19710. https://doi.org/10.1029/2006GL027234

Novello, V. F., Cruz, F. W., Karmann, I., Burns, S. J., Stirkis, N. M., Vuille, M., et al. (2012). Multidecadal climate variability in Brazil's Nordeste during the last 3000 years based on speleothem isotope records. *Geophysical Research Letters*, *39*, L23706. https://doi.org/10.1029/2012GL053936

Novello, V. F., Vuille, M., Cruz, F. W., Stríkis, N. M., Paula, de, M. S., Edwards, R. L., et al. (2016). Centennial-scale solar forcing of the South American Monsoon System recorded in stalagmites. *Scientific Reports*, *6*, 24762. https://doi.org/10.1038/srep24762

Oppo, D. W., Rosenthal, Y., & Linsley, B. K. (2009). 2,000-year-long temperature and hydrology reconstructions from the Indo-Pacific warm pool. *Nature*, *460*, 1113–1116. https://doi.org/10.1038/nature08233

Orrison, R., & Vuille, M. 2020. Dynamical drivers of South American monsoon variability over the last millennium. AGU 2020 Fall Meeting.

Otto-Bliesner, B. L., Brady, E. C., Fasullo, J., Jahn, A., Landrum, L., Stevenson, S., et al. (2016). Climate variability and change since 850 CE: An ensemble approach with the community earth system model. *Bulletin of the American Meteorological Society*, *97*, 735–754. https://doi.org/10.1175/bams-d-14-00233.1

PAGES 2k Consortium (2013). Continental-scale temperature variability during the past two millennia. *Nature Geoscience*, *6*, 339–346.

PAGES 2k Consortium (2019). Consistent multidecadal variability in global temperature reconstructions and simulations over the Common Era. *Nature Geoscience Series*, *12*, 643–649.

PAGES 2k-PMIP3 Group (2015). Continental-scale temperature variability in PMIP3 simulations and PAGES 2k regional temperature reconstructions over the past millennium. *Climate of the Past*, *11*, 1673–1699.

PAGES Hydro2k Consortium (2017). Comparing proxy and model estimates of hydroclimate variability and change over the Common Era. *Climate of the Past*, *13*, 1851–1900.

Phipps, S. J., Rotstayn, L. D., Gordon, H. B., Roberts, J. L., Hirst, A. C., & Budd, W. F. (2012). The CSIRO Mk3L climate system model version 1.0—Part 2: Response to external forcings. *Geoscientific Model Development*, *5*, 649–682. https://doi.org/10.5194/gmd-5-649-2012

Pope, V. D., Gallani, M. L., Rowntree, P. R., & Stratton, R. A. (2000). The impact of new physical parametrizations in the Hadley Centre climate model: HadAM3. *Climate Dynamics*, *16*, 123–146. https://doi.org/10.1007/s003820050009

Raddatz, T. J., Reick, C. H., Knorr, W., Kattge, J., Roeckner, E., Schnur, R., et al. (2007). Will the tropical land biosphere dominate the climate-carbon cycle feedback during the twenty-first century? *Climate Dynamics*, *29*, 565–574. https://doi.org/10.1007/s00382-007-0247-8

Reuter, J., Stott, L., Khider, D., Sinha, A., Cheng, H., & Edwards, R. L. (2009). A new perspective on the hydroclimate variability in northern South America during the Little Ice Age. *Geophysical Research Letters*, *36*. https://doi.org/10.1029/2009GL041051

Richey, J. N., & Sachs, J. P. (2016). Precipitation changes in the western tropical Pacific over the past millennium. *Geology*, *44*, 671–674. https://doi.org/10.1130/g37822.1

Risi, C., Bony, S., & Vimeux, F. (2008). Influence of convective processes on the isotopic composition (delta O-18 and delta D) of precipitation and water vapor in the tropics: 2. Physical interpretation of the amount effect. *Journal of Geophysical Research*, *113*, D19306. https://doi.org/10.1029/2008JD009943

Risi, C., Bony, S., Vimeux, F., & Jouzel, J. (2010). Water-stable isotopes in the LMDZ4 general circulation model: Model evaluation for present-day and past climates and applications to climatic interpretations of tropical isotopic records. *Journal of Geophysical Research*, *115*, D12118. https://doi.org/10.1029/2009JD013255

Roberts, W. H. G., Valdes, P. J., & Singarayer, J. S. (2017). Can energy fluxes be used to interpret glacial/interglacial precipitation changes in the tropics? *Geophysical Research Letters*, *44*, 6373–6382. https://doi.org/10.1002/2017GL073103

Rodbell, D. T., Seltzer, G. O., Anderson, D. M., Abbott, M. B., Enfield, D. B., & Newman, J. H. (1999). An ~15,000-year record of El Niño-driven alluviation in southwestern Ecuador. *Science*, *283*, 516. https://doi.org/10.1126/science.283.5401.516

Rodysill, J. R., Russell, J. M., Bijaksana, S., Brown, E. T., Safiuddin, L. O., & Eggermont, H. (2012). A paleolimnological record of rainfall and drought from East Java, Indonesia during the last 1,400 years. *Journal of Paleolimnology*, *47*, 125–139. https://doi.org/10.1007/s10933-011-9564-3

Rotstayn, L. D., Jeffrey, S. J., Collier, M. A., Dravitzki, S. M., Hirst, A. C., Syktus, J. I., & Wong, K. K. (2012). Aerosol- and greenhouse gas-induced changes in summer rainfall and circulation in the Australasian region: A study using single-forcing climate simulations. *Atmospheric Chemistry and Physics*, *12*, 6377–6404. https://doi.org/10.5194/acp-12-6377-2012

Russell, J. M., Verschuren, D., & Eggermont, H. (2007). Spatial complexity of 'Little Ice Age' climate in East Africa: Sedimentary records from two crater lake basins in western Uganda. *The Holocene*, *17*, 183–193. https://doi.org/10.1177/0959683607075832

Sachs, J. P., Sachse, D., Smittenberg, R. H., Zhang, Z., Battisti, D. S., & Golubic, S. (2009). Southward movement of the pacific intertropical convergence zone AD 1400–1850. *Nature Geoscience*, *2*, 519–525. https://doi.org/10.1038/ngeo554

Schmidt, G. A., Jungclaus, J. H., Ammann, C. M., Bard, E., Braconnot, P., Crowley, T. J., et al. (2011). Climate forcing reconstructions for use in PMIP simulations of the last millennium (v1.0). *Geoscientific Model Development*, *4*, 33–45. https://doi.org/10.5194/gmd-4-33-2011

Schmidt, G. A., Ruedy, R., Hansen, J. E., Aleinov, I., Bell, N., Bauer, M., et al. (2006). Present-day atmospheric simulations using GISS ModelE: Comparison to in situ, satellite, and reanalysis data. *Journal of Climate*, *19*, 153–192. https://doi.org/10.1175/jcli3612.1

Schurer, A. P., Hegerl, G. C., Mann, M. E., Tett, S. F. B., & Phipps, S. J. (2013). Separating forced from chaotic climate variability over the past millennium. *Journal of Climate*, *26*, 6954–6973. https://doi.org/10.1175/jcli-d-12-00826.1

Schurer, A. P., Tett, S. F. B., & Hegerl, G. C. (2014). Small influence of solar variability on climate over the past millennium. *Nature Geoscience*, *7*, 104–108. https://doi.org/10.1038/ngeo2040

Shanahan, T. M., Overpeck, J. T., Anchukaitis, K. J., Beck, J. W., Cole, J. E., Dettman, D. L., et al. (2009). Atlantic forcing of persistent drought in West Africa. *Science*, *324*, 377–380. https://doi.org/10.1126/science.1166352

Shuman, B. N., Routson, C., McKay, N., Fritz, S., Kaufman, D., Kirby, M. E., et al. (2018). Placing the Common Era in a Holocene context: Millennial to centennial patterns and trends in the hydroclimate of North America over the past 2000 years. *Climate of the Past*, *14*, 665–686. https://doi.org/10.5194/cp-14-665-2018

Sigl, M., McConnell, J. R., Toohey, M., Curran, M., Das, S. B., Edwards, R., et al. (2014). Insights from Antarctica on volcanic forcing during the Common Era. *Nature Climate Change*, *4*, 693–697. https://doi.org/10.1038/nclimate2293

Sigl, M., Winstrup, M., McConnell, J. R., Welten, K. C., Plunkett, G., Ludlow, F., et al. (2015). Timing and climate forcing of volcanic eruptions for the past 2,500 years. *Nature*, *523*, 543–549. https://doi.org/10.1038/nature14565

Singarayer, J. S., Valdes, P. J., & Roberts, W. H. G. (2017). Ocean dominated expansion and contraction of the late Quaternary tropical rainbelt. *Scientific Reports*, *7*, 9382. https://doi.org/10.1038/s41598-017-09816-8

Sinha, A., Stott, L., Berkelhammer, M., Cheng, H., Edwards, R. L., Buckley, B., et al. (2011). A global context for megadroughts in monsoon Asia during the past millennium. *Quaternary Science Reviews*, *30*, 47–62. https://doi.org/10.1016/j.quascirev.2010.10.005

Sletten, H. R., Railsback, L. B., Liang, F., Brook, G. A., Marais, E., Hardt, B. F., et al. (2013). A petrographic and geochemical record of climate change over the last 4600 years from a northern Namibia stalagmite, with evidence of abruptly wetter climate at the beginning of southern Africa's Iron Age. *Palaeogeography, Palaeoclimatology, Palaeoecology*, *376*, 149–162. https://doi.org/10.1016/j.palaeo.2013.02.030

Stager, J. C., Ryves, D. B., King, C., Madson, J., Hazzard, M., Neumann, F. H., & Maud, R. (2013). Late Holocene precipitation variability in the summer rainfall region of South Africa. *Quaternary Science Reviews*, *67*, 105–120. https://doi.org/10.1016/j.quascirev.2013.01.022

Stansell, N. D., Steinman, B. A., Abbott, M. B., Rubinov, M., & Roman-Lacayo, M. (2012). Lacustrine stable isotope record of precipitation changes in Nicaragua during the Little Ice Age and Medieval Climate Anomaly. *Geology*, *41*, 151–154. https://doi.org/10.1130/G33736.1

Stott, L., Cannariato, K., Thunell, R., Haug, G. H., Koutavas, A., & Lund, S. (2004). Decline of surface temperature and salinity in the western tropical Pacific Ocean in the Holocene epoch. *Nature*, *431*, 56–59. https://doi.org/10.1038/nature02903

Swingedouw, D., Terray, L., Cassou, C., Voldoire, A., Salas-Mélia, D., & Servonnat, J. (2011). Natural forcing of climate during the last millennium: Fingerprint of solar variability. *Climate Dynamics*, *36*, 1349–1364. https://doi.org/10.1007/s00382-010-0803-5

Tan, L., Cai, Y., An, Z., Edwards, R. L., Cheng, H., Chuan-Chou, S., & Zhang, H. (2010). Centennial- to decadal-scale monsoon precipitation variability in the semi-humid region, northern China during the last 1860 years: Records from stalagmites in Huangye Cave. *The Holocene*, *21*, 287–296. https://doi.org/10.1177/0959683610378880

Taylor, B. L. (2010). *A speleothem-based high resolution reconstruction of climate in Southeastern Brazil over the past 4,100 years*. Department of Geosciences, University of Massachusetts.

Taylor, K. E., Crucifix, M., Braconnot, P., Hewitt, C. D., Doutriaux, C., Broccoli, A. J., et al. (2007). Estimating shortwave radiative forcing and response in climate models. *Journal of Climate*, *20*, 2530–2543. https://doi.org/10.1175/jcli4143.1

Tejedor, E., Steiger, N. J., Smerdon, J. E., Serrano-Notivoli, R., & Vuille, M. (2021). Global hydroclimatic response to tropical volcanic eruptions over the last millennium. *Proceedings of the National Academy of Sciences*, *118*, e2019145118. https://doi.org/10.1073/pnas.2019145118

Thompson, L. G., Mosley-Thompson, E., Davis, M. E., Zagorodnov, V. S., Howat, I. M., Mikhalenko, V. N., & Lin, P. N. (2013). Annually resolved ice core records of tropical climate variability over the past ~1800 years. *Science*, *340*, 945. https://doi.org/10.1126/science.1234210

Tierney, J. E., Abram, N. J., Anchukaitis, K. J., Evans, M. N., Giry, C., Kilbourne, K. H., et al. (2015). Tropical sea surface temperatures for the past four centuries reconstructed from coral archives. *Paleoceanography*, *30*, 226–252. https://doi.org/10.1002/2014PA002717

Tierney, J. E., Oppo, D. W., Rosenthal, Y., Russell, J. M., & Linsley, B. K. (2010). Coordinated hydrological regimes in the Indo-Pacific region during the past two millennia. *Paleoceanography*, *25*, PA1102. https://doi.org/10.1029/2009PA001871

Toohey, M., & Sigl, M. (2017). Volcanic stratospheric sulfur injections and aerosol optical depth from 500 BCE to 1900 CE. *Earth System Science Data*, *9*, 809–831. https://doi.org/10.5194/essd-9-809-2017

Toomey, M. R., Donnelly, J. P., & Tierney, J. E. (2016). South Pacific hydrologic and cyclone variability during the last 3000 years. *Paleoceanography*, *31*, 491–504. https://doi.org/10.1002/2015PA002870

Vuille, M., Burns, S. J., Taylor, B. L., Cruz, F. W., Bird, B. W., Abbott, M. B., et al. (2012). A review of the South American monsoon history as recorded in stable isotopic proxies over the past two millennia. *Climate of the Past*, *8*, 1309–1321. https://doi.org/10.5194/cp-8-1309-2012

Vuille, M., & Werner, M. (2005). Stable isotopes in precipitation recording South American summer monsoon and ENSO variability: Observations and model results. *Climate Dynamics*, *25*, 401–413. https://doi.org/10.1007/s00382-005-0049-9

Wallace, J. M., Rasmusson, E. M., Mitchell, T. P., Kousky, V. E., Sarachik, E. S., & Storch, von, H. (1998). On the structure and evolution of ENSO-related climate variability in the tropical Pacific: Lessons from TOGA. *Journal of Geophysical Research*, *103*, 14241–14259. https://doi.org/10.1029/97JC02905

Wang, L., Sarnthein, M., Grootes, P. M., & Erlenkeuser, H. (1999). Millennial reoccurrence of century-scale abrupt events of East Asian Monsoon: A possible heat conveyor for the global deglaciation. *Paleoceanography*, *14*, 725–731.

Wang, Y., Cheng, H., Edwards, R. L., He, Y. Q., Kong, X. G., An, Z. S., et al. (2005). The Holocene Asian monsoon: Links to solar changes and North Atlantic climate. *Science*, *308*, 854–857. https://doi.org/10.1126/science.1106296

Wodzicki, K. R., & Rapp, A. D. (2016). Long-term characterization of the Pacific ITCZ using TRMM, GPCP, and ERA-Interim. *Journal of Geophysical Research: Atmospheres*, *121*, 3153–3170. https://doi.org/10.1002/2015JD024458

Yan, H., Sun, L., Wang, Y., Huang, W., Qiu, S., & Yang, C. (2011). A record of the southern oscillation index for the past 2,000 years from precipitation proxies. *Nature Geoscience*, *4*, 611–614. https://doi.org/10.1038/ngeo1231

Yan, H., Wei, W., Soon, W., An, Z., Zhou, W., Liu, Z., et al. (2015). Dynamics of the intertropical convergence zone over the western pacific during the little ice age. *Nature Geoscience*, *8*, 315–320. https://doi.org/10.1038/ngeo2375

Zhang, P., Cheng, H., Edwards, R. L., Chen, F., Wang, Y., Yang, X., et al. (2008). A test of climate, sun, and culture relationships from an 1810-year Chinese cave record. *Science*, *322*, 940–942. https://doi.org/10.1126/science.1163965

Zhao, K., Wang, Y., Edwards, R. L., Cheng, H., Liu, D., & Kong, X. (2015). A high-resolved record of the Asian Summer Monsoon from Dongge Cave, China for the past 1200 years. *Quaternary Science Reviews*, *122*, 250–257. https://doi.org/10.1016/j.quascirev.2015.05.030